Master Thesis, Department of Geosciences

Compensation of Absorption Effects in Seismic Data

Hagos Geberehiwet Gebregergs

UNIVERSITY OF OSLO

FACULTY OF MATHEMATICS AND NATURAL SCIENCES

Compensation of Absorption Effects in Seismic Data

Hagos Gebrehiwet Gebregergs

Master Thesis in Geosciences

Discipline: Geophysics

Department of Geosciences

Faculty of Mathematics and Natural Sciences

University of Oslo

Spring 2016

Abstract

The frequency content of seismic data is changing with propagation depth due to intrinsic absorption. This implies that the higher frequencies are highly attenuated, thus leading to a loss in resolution of the seismic image. In addition, absorption anomalies, for example, caused by gas sands, will further dim the seismic reconstruction.

The absorptive property of a medium can be described by a quality factor Q, which determines the energy decay and a velocity dispersion relationship. The quality factor and the velocity govern the propagation of seismic energy in the earth.

It is possible to correct for such absorption effects by employing so-called inverse Q-filtering (IQF). This is a filtering technique that tries to restore the loss of the higher frequencies due to propagation. Newer developments within IQF can be regarded as a migration type of algorithm, and such classes of techniques are studied in this thesis.

Keywords: Absorption compensation, Quality factor Q and Q-model, Absorption function $Y(\omega, \tau)$, Forward Q modelling, Inversion, Reflectivity, Reflectivity per depth unit.

Contents

Chapter 1

Introduction

As seismic waves travel through the earth, the visco-elasticity of the earth's medium will cause energy dissipation and waveform distortion. This phenomenon is referred to as seismic absorption.

High frequencies are more attenuated than low frequencies, and that this reduces resolution. We want therefore to try to remove the effect of absorption. In seismic data processing, absorption can be compensated for to enhance seismic data resolution. In hydrocarbon reservoir description, seismic absorption can be used as an important attribute to interpret for fluid units.

1.1 Statement of Problem

The research being presented in this thesis deals with compensation of absorption effects in seismic data by employing so-called inverse Q-filtering (IQF). This is a filtering technique that tries to restore the loss of higher frequencies due to propagation. Relevant migration type algorithms (linear and non-linear IQF) will be studied in this thesis. These IQF techniques will be implemented in Matlab.

1.2 Seismic Wave and Absorption Phenomena

Seismic method utilizes the propagation of waves through the earth which depends upon the elastic properties of the rocks within the subsurface. A seismic wave is shot to the earth's subsurface. Part of the shot energy is reflected back. The reflection happens due to difference in acoustic impedance, the product of wave velocity and density, across an interface in the subsurface. The reflected seismic data is processed to give seismic image of the subsurface. The seismic image is interpreted to explore the physical properties of the rocks within and the structural information of the subsurface. However, the seismic interpretation depends on the resolution of the seismic image which also depends on the quality of the seismic data and processing techniques.

Propagation of seismic wave is affected by the anelasticity and heterogeneity of the earth's subsurface. As a result, seismic waves get absorbed while propagating through the earth's subsurface, (Futterman 1962, Kjartansson 1979, Kolsky 1956, Ricker 1953, Strick 1967). The absorption of seismic waves in the earth's subsurface causes both amplitude attenuation and velocity dispersion of the reflections recorded on the surface, which are interrelated, leading to a loss of resolution thereby resulting in loss of information concerning targets of potential interest. This absorptive property is often represented by a quality factor Q, which is an intrinsic property of rocks. According to Futterman (1962), the quality factor Q, is defined as a dimensionless measure of the anelasticity which is given by

$$\frac{1}{Q} = \frac{|\triangle E|}{2\pi E_0} \approx \frac{2\alpha(\omega)v(\omega)}{\omega}, \tag{1.1}$$

where E_0 is the energy stored at the maximum strain in a volume, $\triangle E$ is the energy loss in each cycle because of anelasticity, ω angular frequency, $\alpha(\omega)$ amplitude attenuation coefficient and $v(\omega)$ phase velocity of the seismic wave. Equation (1.1) implies that Q^{-1} is the portion of energy lost during each cycle or wavelength.

As the seismic wave passes through the medium in the subsurface, the elastic energy associated with the wave motion is gradually absorbed by the medium, reappearing ultimately in the form of heat. This process is responsible for the eventual complete disappearance of the wave motion. Internal friction, piezoelectric and thermoelectric effects, and viscous fluid flow loss of the fluids filling the rock pores are among the mechanisms by which the elastic energy is transformed into other forms of energy such as heat, (Johnston et al. 1979, Mavko et al. 1979, Ricker 1977, Telford et al. 1991, White 1975).

Because seismic absorption has a considerable impact on amplitude and wave shape in recorded seismic data, it is of particular importance when seismic attributes and inversion schemes are required to extract lithological information, porosity, permeability, viscosity and degree of saturation of rocks. Since rocks in the earth's subsurface are almost always fluid saturated with brine, oil and gas, it is possible that fluid related mechanism might easily dominate dry rock sources of absorption, (Barton 2007, Biot 1956*a*,*b*, Gelius & Johansen 2012, Mavko & Nur 1979).

Gelius (1987) showed that application of inverse Q filtering on field data from a shallow gas reservoir in the North Sea generally improved the resolution, and improved the match between the synthetic and the field data on both sides of the well. In order to recover a weak reflection of a target gas-layer underneath a strong coal-seam reflections, Wang & Guo (2004*b*) were able to show improvement of vertical resolution in migrated seismic sections applying migration with inverse Q filtering algorithm in a real data. In Wang (2008) it is shown that application of inverse Q filter on real seismic data resulted in better matching of seismic impedance sections and well-log information, enhanced seismic resolution of a potential target reservoir, and better reservoir

characterization like lateral heterogeneity of a carbonate gas reservoir. In Oliveira & Lupinacci (2013) it is shown that inversion was capable of raising the resolution of real data that was affected by shallow gas accumulations without boosting the noise present in the data.

1.3 Methods of Absorption Compensation

To remove the effect of absorption, the most common ones are time-variant spectral whitening, time-variant deconvolution and inverse Q filtering, (Gelius 1987, Hale 1982, Hargreaves & Calvert 1991, Montaña & Margrave 2004, Nilsen & Gjevik 1978, Wang 2006, Yilmaz 2001). Time-variant spectral whitening tries to recover the lost high-frequency energy by applying an exponential gain function to the seismic data divided into frequency bands. Time-variant deconvolution implements absorption compensation by means of a time-variant wavelet in a moving time window. Inverse Q filtering is a deterministic process that requires knowledge of the quality factor Q. The chief difficulty to absorption compensation lies on the nonstationary characteristics generated by the absorption process in the seismic traces recorded. In an attenuating medium, the shape of seismic pulse wavelet recorded in the beginning of the trace will differ from the wavelet's shape recorded in the later times of the signal.

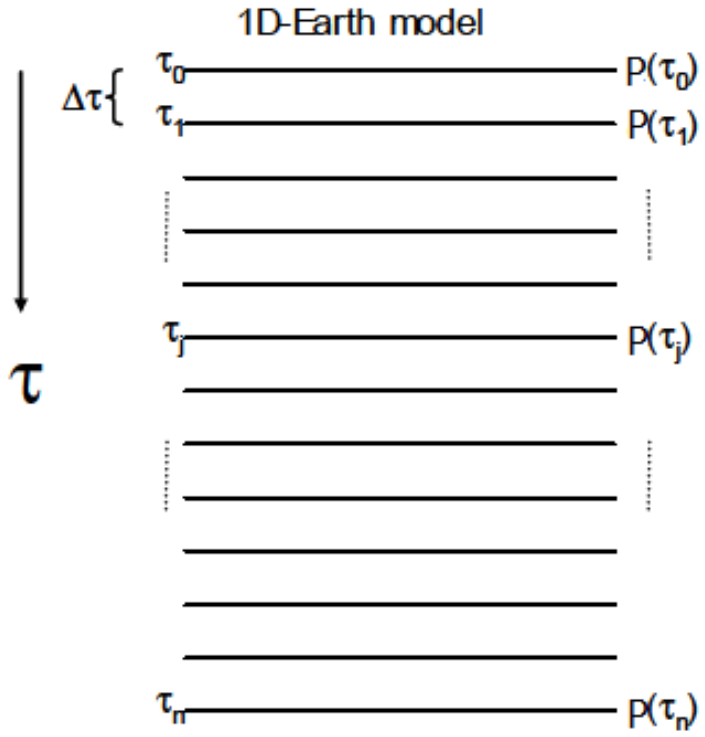

FIGURE 1.1: Inverse Q filter by downward continuation of a 1-D layered earth model, where τ is two-way traveltime and $P(\tau)$ is plane pressure wave at depth τ. (Adapted from Montaña & Margrave (2004).)

Inverse Q filtering algorithms are mainly based on downward wave propagation migration type approach, where the decay of the frequency content due to absorption can be inspected at each time sample, (Bickel & Natarajan 1985, Hargreaves & Calvert 1991, Montaña & Margrave 2004, Wang 2002, 2006). That is, a pressure wavefield $P(\omega, \tau+\triangle\tau)$ at time step $\triangle\tau$ later, shown in figure 1.1, can be computed as:

$$P(\omega, \tau + \triangle\tau) = P(\omega, \tau) \exp\big[- i\tilde{k}\triangle\tau\big], \tag{1.2}$$

where τ is two-way traveltime for depth, ω is frequency and $\tilde{k}$ is complex-valued wavenumber.

There are stability and signal-to-noise ratio (S/N) issues with these inverse Q filtering algorithms as we move to the high frequency bands. Usually, the dispersion and amplitude corrections are dealt separately. This is because these inverse Q filters are easily separated into both phase-only and amplitude-only components. That is, with complex-valued wavenumber $\tilde{k}$:

$$\tilde{k} = \frac{\omega}{v(\omega)}\left[1 - \frac{i}{2Q}\right], \tag{1.3}$$

the wavefield at the surface $P(\omega, 0)$ is extrapolated down to $P(\omega, \tau)$ at depth τ,

$$P(\omega, \tau) = P(\omega, 0) \exp\left[- \frac{\omega\tau}{2Qv(\omega)}\right] \exp\left[- i\frac{\omega\tau}{v(\omega)}\right] \tag{1.4}$$

where $v(\omega)$ is the phase velocity of the wave and Q is the quality factor of the medium of propagation. The first exponent in equation (1.4) describes all amplitude attenuation and the second exponent describes all dispersion effects. Moreover, dispersion corrections of seismic data based on phase-only inverse Q filtering is inherently stable process as no energy is boosted, but solely involves phase changes. On the other hand, attenuation corrections based on amplitude-only inverse Q filtering leads to noise amplification as well as bandwidth enhancement which raises the stability issue, (van der Baan 2012).

A slightly different approach of "Inversion of Reflection Data" is presented by Nilsen & Gjevik (1978). Nilsen and Gjevik solved the non-linear wave equation for a pressure wave by introducing an absorption function $\Theta = \Theta(\alpha, \rho, \eta, k, \omega)$, a complex function of absorption coefficient α, density ρ, viscosity η, wave number k and frequency ω. Similarly a layered earth model is implemented to solve the non-linear wave equation by introducing absorption function $Y(\omega, \tau)$, where two way traveltime τ and frequency ω. In an inversion problem the coefficients of the reflectivity series are the parameter to be estimated. The main advantage of this approach is that it is very robust to the presence of noise; since the solution is obtained by minimizing a misfit between observed and modelled data, (Oliveira & Lupinacci 2013).

1.4 Thesis Structure

In Chapter 1, we have communicated the background of the research on seismic absorption. Absorption phenomenon is explained. The need and possible mechanisms of absorption compensation are presented. A connection between the goal of this thesis and similar previous work is identified. Difference between inverse Q filtering algorithms based on downward wave propagation migration type approach and inversion is introduced.

Chapter 2 presents in detail the mathematical descriptions and modelling of seismic absorption compensation. To include the medium absorption effects that are both wave amplitude attenuation and velocity dispersion, an absorption function of the form $Y(\omega,\tau) = A(\omega,\tau) + iB(\omega,\tau)$, (Horton 1959), is introduced into the functional relationship between a stress and strain fields of a pressure stress. Combining with equation of motion of the pressure stress, a non-linear seismic wave equation is derived and solved iteratively by finite difference method. The absorption function $Y(\omega,\tau) = A(\omega,\tau) + iB(\omega,\tau)$ of Futterman (1962) and Wang & Guo (2004*a*) Q dispersion models is derived.

In chapter 3 different results of the developed Matlab algorithm are displayed and explained. First forward Q modelling of both linear and non-linear effects are discussed. Synthetic seismograms with and without multiples are produced using the different Q dispersion models: Kolsky (1956) combined with Kjartansson (1979) and alternative Futterman (1962) as well as dispersionless Q-model. Differences and similarities of the results of these Q dispersion models are discussed. After the forward modelling of the seismogram of layered 1D earth model, inversion is performed to calculate a reflectivity per depth series by using the synthetic seismogram as an input.

In chapter 4, results of inversion are presented and discussed. As the forward Q modelled synthetic seismogram is used as input, a different Q-value is used during inversion process to explore the effects of wrong Q-value. The same procedure is repeated using a different Q-model to explore the effects of Q-model. Finally, chapter 5 gives discussion and conclusion.

Chapter 2

Modelling of Absorption Compensation

Seismic wave traveling in the earth experience amplitude attenuation and velocity dispersion due to the absorptive property of the rocks of the subsurface. This absorptive behavior of earth can be modelled where each layer of the earth is described by layer thickness z, velocity v, density ρ and a quality factor Q.

2.1 Q Dispersion Models

When using Q to describe seismic attenuation, it is often assumed that Q does not change with frequency in the seismic frequency range (10 - 200Hz). A good understanding of the mathematical Q-models is necessary for design and application of an inverse Q filtering algorithm. The seismic amplitude varies with depth z because of attenuation such that

$$A(z) = A(0) \exp\big[-\alpha(\omega) z\big], \tag{2.1}$$

where $A(0)$ is the seismic amplitude at the source ($z = 0$). The attenuation coefficient $\alpha(\omega)$ is linear in frequency, that is

$$\alpha(\omega) = \frac{|\omega|}{2 v_r Q}, \tag{2.2}$$

where v_r is the propagation velocity at a reference frequency ω_r. This part is common to all Q-models. It is more complicated to describe the dispersion and there are different Q-models for that. Kolsky (1956), Futterman (1962) and Kjartansson (1979) have developed various Q-models to describe the velocity dispersion. They use different approaches leading to the general form for the frequency dependence of the phase velocity $v(\omega)$, which is valid for large and constant quality factor Q:

$$\frac{1}{v(\omega)} = \frac{1}{v_r}\left[1 - \frac{1}{\pi Q} \ln\left|\frac{\omega}{\omega_r}\right|\right], \tag{2.3}$$

In Kjartansson (1979), the frequency dependence of Q is assumed to be insignificant over the range of seismic frequency and first order Taylor expansion:

$$\frac{1}{v_r}\left[1-\frac{1}{\pi Q}\ln\left|\frac{\omega}{\omega_r}\right|\right]\approx\frac{1}{v_r}\left|\frac{\omega}{\omega_r}\right|^{-\frac{1}{\pi Q}},\quad\text{for}\quad Q\gg 1. \tag{2.4}$$

It is a good representation of the attenuation process for most crustal rocks in the range of useful frequencies for seismic processing.

2.2 Non-Linear Modelling with Absorption

For most absorption mechanisms that are significant in rocks, irrespective of the microstructure of the rocks in the earth's subsurface, the phenomenological aspects of seismic wave propagation can be treated relatively independent of the details of the particular physical mechanisms responsible for the energy absorption. To obtain realistic and accurate modelling results for wave propagation, Q absorption should be incorporated into modelling algorithm appropriately, and this can be done either in frequency domain or time domain. Usually, it is more convenient to account for Q absorption in frequency domain.

In order to apply forward modelling and deduce an inversion method which is based on an iterative solution of the seismic wave equation while incorporating the amplitude attenuation and velocity dispersion in the complex-valued wavenumber $\tilde{k}(\omega)$ implicitly through the earth's subsurface quality factor Q, a plane parallel stratification with no lateral inhomogeneities is assumed. The equation of motion of a plane pressure stress pulse, propagating through a medium where the density ρ and seismic velocity v vary gradually with depth, in a frequency domain is

$$\frac{\partial P}{\partial z}=-\rho\omega^2 W, \tag{2.5}$$

where W and P denote the displacement and pressure stress in the z-direction. Gjevik et al. (1976) assumed the functional relation between the stress and the strain fields to be linear and isotropic as

$$P=\rho v^2\frac{\partial W}{\partial z}. \tag{2.6}$$

The wave speed of the propagating pressure stress depends on the medium elastic parameters λ and μ as in

$$v=\sqrt{\frac{\lambda+2\mu}{\rho}}. \tag{2.7}$$

However, equation (2.6) does not include the absorption aspect of the seismic wave propagation. Therefore, Nilsen & Gjevik (1978) corrected for the absorption effect by assuming Kelvin Voigt model, Jaeger (1962), stress-strain

relationship

$$P = \rho v^2 \Theta^2 \frac{\partial W}{\partial z}, \tag{2.8}$$

with $\Theta = \Theta(\alpha, \rho, \eta, k, \omega)$ is being a complex-valued function of absorption coefficient α, density ρ, viscosity η, wave number k and frequency ω.

In this thesis, an absorption function $Y(\omega, \tau)$ has been introduced in the stress and strain relationship as

$$P = \rho v_r^2 Y \frac{\partial W}{\partial z}, \tag{2.9}$$

where v_r is the reference velocity which could be taken as group velocity in the case of dispersion. The absorption function $Y(\omega, \tau)$ depends on depth (measured in two way traveltime τ) and frequency ω, with $Y = 1$ being absorption free as in equation (2.6) by Gjevik et al. (1976). Therefore, combining equations (2.5) and (2.9) give Helmholtz equation, assuming constant density which is in agreement with the layered approach in this thesis:

$$\frac{\partial^2 P}{\partial z^2} + \tilde{k}^2 P = 0, \qquad \tilde{k} = \frac{\omega}{v_r \sqrt{Y}}, \tag{2.10}$$

with $\tilde{k}$ being a complex-valued wavenumber.

2.3 Absorption Function and Q Models

Following Horton (1959), we introduced the notation

$$Y(\omega, \tau) = A(\omega, \tau) + iB(\omega, \tau). \tag{2.11}$$

In this paper, Horton (1959) gives examples of values of A and B for various absorption models (not necessarily causal ones!). In this thesis the different absorption compensation models are results of the corresponding Q models. Since the complex-valued wavenumber $\tilde{k}$ is in focus which in turn gives the absorption function $Y(\omega, \tau) = A(\omega, \tau) + iB(\omega, \tau)$ corresponding to the different Q-models, the following expression is now elaborated on by first order Taylor expansion:

$$\begin{aligned} \frac{1}{\sqrt{Y}} &= \frac{1}{\sqrt{A + iB}} = A^{-1/2}\left[1 + i\frac{B}{A}\right]^{-1/2} \cong A^{-1/2}\left[1 - i\frac{B}{2A}\right] \quad \text{for} \quad A \gg B, \\ \tilde{k} &= \frac{\omega}{v_r \sqrt{Y}} = \frac{\omega}{v_r \sqrt{A + iB}} \cong \frac{\omega}{v_r}\left[\frac{1}{\sqrt{A}} - \frac{i}{2}\frac{B}{A\sqrt{A}}\right]. \end{aligned} \tag{2.12}$$

In the literature the complex-valued wavenumber $\tilde{k}$ is often written on the following form in case of absorption (constant-Q model):

$$\begin{aligned} \tilde{k} &= \frac{\omega}{v(\omega)}\left[1 - \frac{i}{2Q}\right] = \frac{\omega}{v_r} + \left[\frac{\omega}{v(\omega)} - \frac{\omega}{v_r}\right] - i\alpha(\omega), \\ &= \frac{\omega}{v_r} + \varphi(\omega) - i\alpha(\omega), \qquad \alpha(\omega) = \frac{\omega}{2Qv(\omega)}, \end{aligned} \tag{2.13}$$

where α is the absorption coefficient and φ is the phase of the 'absorption filter'. In order to ensure causality, this filter should be minimum phase. For such a filter this relationship holds

$$\varphi(\omega) = \aleph\big[\alpha(\omega)\big], \tag{2.14}$$

with $\aleph$ denoting the Hilbert Transform. If we omit dispersion (put $\varphi = 0$), the filter will be non-causal. Equating equations (2.12) and (2.13) gives the relationships

$$A = \left[\frac{v(\omega)}{v_r}\right]^2, \qquad B = \left[\frac{v(\omega)}{v_r}\right]^2 \frac{1}{Q}. \tag{2.15}$$

Aki & Richards (2002) show that the following relation should be held to honor causality

$$\frac{\omega}{v(\omega)} - \frac{\omega}{v_\infty} = \aleph\left[\frac{\omega}{2Qv_\infty}\right], \tag{2.16}$$

where v_∞ is the limit of the velocity function when ω tends to infinity. Equation (2.16) can be further approximated as

$$\frac{\omega}{v(\omega)} - \frac{\omega}{v_h} = \aleph\left[\frac{\omega}{2Qv_h}\right], \tag{2.17}$$

where v_h is the velocity related to the highest possible (tuning) frequency of the seismic band, Wang & Guo (2004*a*). The complex-valued wavenumber is accordingly adjusted as (compare with equation (2.13))

$$\tilde{k} = \frac{\omega}{v_h} + \left[\frac{\omega}{v(\omega)} - \frac{\omega}{v_h}\right] - i\frac{\omega}{2Qv(\omega)} = \frac{\omega}{v_h}\left\{1 + \left[\frac{v_h}{v(\omega)} - 1\right] - i\frac{v_h}{2Qv(\omega)}\right\} \tag{2.18}$$

and combined with a Kolsky (1956) type of phase-velocity model of frequency independent Q (constant Q)

$$v(\omega) = v_h\left(\frac{\omega}{\omega_h}\right)^\gamma, \qquad \gamma = (\pi Q)^{-1} \tag{2.19}$$

gives the complex-valued wavenumber model

$$\tilde{k} = \frac{\omega}{v_h}\left\{1 + \left[\left(\frac{\omega}{\omega_h}\right)^{-\gamma} - 1\right] - i\frac{1}{2Q}\left(\frac{\omega}{\omega_h}\right)^\gamma\right\}, \tag{2.20}$$

which has been employed by Wang & Guo (2004*a*). From equations (2.15) and (2.19) it also follows that ($v_r = v_h$)

$$A_{Wang} = \left[\frac{\omega}{\omega_h}\right]^{2\gamma}, \qquad B_{Wang} = \left[\frac{\omega}{\omega_h}\right]^{2\gamma} \frac{1}{Q}. \tag{2.21}$$

From equation (2.21) it follows that $0 < A_{Wang} < 1$, and the same for B_{Wang} but with $B_{Wang} < (<) A_{Wang}$.

Based on equations (2.16) and (2.2), Futterman (1962) proposed an alternative complex-valued wavenumber model

$$\tilde{k} = \frac{\omega}{v_r} + \left[\frac{\omega}{v(\omega)} - \frac{\omega}{v_r}\right] - i\frac{\omega}{2Qv(\omega)} \approx \frac{\omega}{v_r} + \aleph\left[\frac{\omega}{2Qv_r}\right] - i\frac{\omega}{2Qv_r}. \tag{2.22}$$

Based on equations (2.15) and (2.22) it follows that ($v_r = v_\infty$)

$$A_{Futt} = \left[1 + \frac{1}{\omega}\aleph\left(\frac{\omega}{2Q}\right)\right]^2, \qquad B_{Futt} = A_{Futt}^{3/2}\frac{1}{Q}. \tag{2.23}$$

Finally, the dispersion-free and non-causal absorption Q model, i.e. $v(\omega) = v_r$, corresponds to

$$A_{no-disp} = 1, \qquad B_{no-disp} = \frac{1}{Q}. \tag{2.24}$$

2.4 Plane Wave Solutions

In case of a layer/medium with constant velocity and absorption function Y, plane-wave solutions of equation (2.10) can be written formally on the simple form (positive z-axis pointing downwards)

$$U(\omega, z) = a\exp[i\tilde{k}z], \qquad D(\omega, z) = b\exp[-i\tilde{k}z], \qquad \tilde{k} \equiv k - i\alpha\ (k,\ \alpha \geq 0) \tag{2.25}$$

with $U(\omega, z)$ and $D(\omega, z)$ representing respectively upward and downward propagating components. Thus, the total field can be written

$$P = U + D. \tag{2.26}$$

From equation (2.5) and by using equations (2.25) and (2.26) as well as the expression of $\tilde{k}$ from equation (2.10) gives it follows that

$$\begin{aligned} \frac{\partial P}{\partial z} &= \frac{\partial U}{\partial z} + \frac{\partial D}{\partial z} = i\tilde{k}U - i\tilde{k}D = -i\tilde{k}[D - U], \\ W &= -\frac{1}{\rho\omega^2}\frac{\partial P}{\partial z} = \frac{i}{\omega\rho v_r\sqrt{Y}}[D - U]. \end{aligned} \tag{2.27}$$

A depth-varying model can be assumed as the limit of an infinite number of infinitesimal layers. For such a model where the acoustic impedance and the absorption function weakly inhomogeneous compared to the wavelength of the wave, the relation in equation (2.27) is also assumed to be valid, (Nilsen & Gjevik 1978). While making use of equation (2.9), differentiation of equation (2.27) with respect to z gives

$$\begin{aligned} \frac{\partial W}{\partial z} &= \frac{1}{\rho v_r^2 Y}P = \frac{1}{\rho v_r^2 Y}[U + D], \\ &= \frac{i}{\omega\rho v_r\sqrt{Y}}\left[\frac{\partial D}{\partial z} - \frac{\partial U}{\partial z}\right] + \frac{i}{\omega}[D - U]\frac{\partial}{\partial z}\left[\frac{1}{\rho v_r\sqrt{Y}}\right]. \end{aligned} \tag{2.28}$$

Consider now the last term on the right-hand-side (RHS) of equation (2.28), a further simplification can be obtained by considering small to moderate absorption:

$$\frac{\partial}{\partial z}\left[\frac{1}{\rho v_r\sqrt{Y}}\right] = -\frac{1}{\rho v_r\sqrt{Y}}\left[\frac{1}{\sqrt{Y}}\frac{\partial\sqrt{Y}}{\partial z} + \frac{1}{\rho v_r}\frac{\partial(\rho v_r)}{\partial z}\right].$$

For small to moderate absorption, $\frac{1}{\rho v_r}\frac{\partial[\rho v_r]}{\partial z} \gg \frac{1}{\sqrt{Y}}\frac{\partial\sqrt{Y}}{\partial z}$:

$$\frac{\partial}{\partial z}\left[\frac{1}{\rho v_r\sqrt{Y}}\right] \cong -\frac{1}{\rho v_r\sqrt{Y}}\left[\frac{1}{\rho v_r}\frac{\partial(\rho v_r)}{\partial z}\right] = -\frac{2}{\rho v_r\sqrt{Y}}\Upsilon(z), \tag{2.29}$$

$$\Upsilon(z) = \frac{1}{2\rho v_r}\frac{\partial[\rho v_r]}{\partial z}, \tag{2.30}$$

where $\Upsilon(z)$ represents the depth-dependent 'reflectivity' (reflectivity per depth unit). The approximation $\frac{1}{\rho v_r}\frac{\partial[\rho v_r]}{\partial z} \gg \frac{1}{\sqrt{Y}}\frac{\partial\sqrt{Y}}{\partial z}$ holds for low frequency waves in reflection studies of rocks and sediments, (Nilsen & Gjevik 1978). Therefore, using equation (2.29), equation (2.28) can be rearranged to give

$$\frac{\partial D}{\partial z} - \frac{\partial U}{\partial z} = -\frac{i\omega}{v_r\sqrt{Y}}[D+U] + 2\Upsilon(z)[D-U]. \tag{2.31}$$

Similarly, combination of equations (2.5) and (2.26) gives

$$\frac{\partial P}{\partial z} = -\rho\omega^2 W \quad \Longrightarrow \quad \frac{\partial D}{\partial z} + \frac{\partial U}{\partial z} = -\frac{i\omega}{v_r\sqrt{Y}}[D-U]. \tag{2.32}$$

And a main result is obtained now by combining equations (2.31) and (2.32),

$$\begin{aligned}\frac{\partial D}{\partial z} &= -\frac{i\omega}{v_r\sqrt{Y}}D + \Upsilon(z)[D-U],\\ \frac{\partial U}{\partial z} &= \frac{i\omega}{v_r\sqrt{Y}}U - \Upsilon(z)[D-U].\end{aligned} \tag{2.33}$$

To solve the above coupled equations (2.33), let us now introduce the earth's response described by the ratio $K = U/D$, (Yilmaz 2001), and differentiate it with respect to depth

$$\frac{\partial K}{\partial z} = \frac{\partial[U/D]}{\partial z} = \frac{1}{D}\frac{\partial U}{\partial z} - \frac{U}{D^2}\frac{\partial D}{\partial z}. \tag{2.34}$$

Finally, by combining equations (2.33) - (2.34) gives the Ricatti equation, (Nilsen & Gjevik 1978),

$$\frac{\partial K}{\partial z} = \frac{2i\omega}{v_r\sqrt{Y}}K - \Upsilon[1-K^2]. \tag{2.35}$$

$K(\omega, z)$ may be interpreted as a complex-valued reflection coefficient which also carries information about the phase delay between the upcoming $U(\omega, z)$ and downgoing $D(\omega, z)$ signals, (Nilsen & Gjevik 1978).

Since vertically traveling waves are considered, the transformation from depth to two-way traveltime is straightforward

$$\begin{aligned} \tau &= 2\int_0^z \frac{dz}{v_r}, \qquad \Rightarrow d\tau = \frac{2}{v_r}dz \quad \text{and} \quad \frac{\partial}{\partial z} = \frac{2}{v_r}\frac{\partial}{\partial \tau}, \qquad (2.36) \\ \Upsilon(z) &= \frac{1}{2\rho v_r}\frac{\partial[\rho v_r]}{\partial z} \equiv \frac{1}{2\rho v_r}\left[\frac{2}{v_r}\frac{\partial[\rho v_r]}{\partial \tau}\right] = \frac{2}{v_r}\left[\frac{1}{2\rho v_r}\frac{\partial[\rho v_r]}{\partial \tau}\right] = \frac{2}{v_r}r(\tau), \\ &\Longrightarrow \quad r(\tau) = \frac{1}{2\rho v_r}\frac{\partial[\rho v_r]}{\partial \tau}, \qquad (2.37) \end{aligned}$$

which gives the traveltime-version of equation (2.35)

$$\begin{aligned} \frac{2}{v_r}\frac{\partial K(\omega,\tau)}{\partial \tau} &= \frac{2i\omega}{v_r\sqrt{Y(\omega,\tau)}}K(\omega,\tau) - \frac{2}{v_r}r(\tau)[1-K^2(\omega,\tau)], \\ \frac{\partial K(\omega,\tau)}{\partial \tau} &= \frac{i\omega}{\sqrt{Y(\omega,\tau)}}K(\omega,\tau) - r(\tau)[1-K^2(\omega,\tau)]. \qquad (2.38) \end{aligned}$$

Equation (2.38) is a non-linear wave equation due to multiples included as a result of weak acoustic impedance contrast of layers in the model. Its solution is the starting point of the forward and inversion algorithms. It should be solved in order to apply for a stratified earth with N layers defined by a two-way traveltimes τ_j, for $j = 0, 1, ..., N-1$, with $\tau_0 = 0$ and τ_N being the maximum record. In case of the forward modelling, the plane-wave upward continuation from the top of the jth layer to surface can be implemented recursively. The presence of absorption function $Y(\omega,\tau)$ in the non-linear wave equation is a necessary and sufficient condition for accounting for the presence of amplitude attenuation and velocity dispersion.

2.5 Forward Q Modelling - Non-Linear Case

If the second part of right-hand-side (RHS) of equation (2.38) is small (or zero) then we are left with linear and homogenous differential equation:

$$\frac{\partial K(\omega,\tau)}{\partial \tau} = \frac{i\omega}{\sqrt{Y(\omega,\tau)}}K(\omega,\tau), \qquad (2.39)$$

where the solution is

$$K(\omega,\tau) = K(\omega,0)\exp\left[\int_0^\tau \frac{i\omega}{\sqrt{Y(\omega,\tau')}}\partial\tau'\right]. \qquad (2.40)$$

Therefore, we can look for a solution of equation (2.38) of the form

$$K(\omega,\tau) = C(\tau)\exp\left[\int_0^\tau \frac{i\omega}{\sqrt{Y(\omega,\tau')}}\partial\tau'\right], \qquad (2.41)$$

where

$$C(\tau) = K(\omega,\tau)\exp\left[-\int_0^\tau \frac{i\omega}{\sqrt{Y(\omega,\tau')}}\partial\tau'\right], \quad (2.42)$$

$$= K(\omega,\tau)\exp\left[-i\Phi(\omega,\tau)\right],$$

$$\Phi(\omega,\tau) = \int_0^\tau \frac{\omega}{\sqrt{Y(\omega,\tau')}}\partial\tau' \cong \int_0^\tau \left[\frac{\omega}{\sqrt{A}} - \frac{i\omega B}{A\sqrt{A}}\right]\partial\tau', \quad (2.43)$$

and expect $C(\tau)$ to vary more slowly than the exponential and therefore be easier to calculate.

Differentiating both sides of equation (2.42) we get

$$\frac{\partial C(\tau)}{\partial\tau} = \left[\frac{\partial K(\omega,\tau)}{\partial\tau} + \frac{-i\omega}{\sqrt{Y(\omega,\tau)}}K(\omega,\tau)\right]\exp\left[-\int_0^\tau \frac{i\omega}{\sqrt{Y(\omega,\tau')}}\partial\tau'\right]. \quad (2.44)$$

Substituting $\partial K(\omega,\tau)/\partial\tau$ of equation (2.38) in equation (2.44) we get the rewritten Riccati equation on the following form:

$$\frac{\partial}{\partial\tau}\left[K(\omega,\tau)\exp\left[-i\Phi(\omega,\tau)\right]\right] = -r(\tau)\left[1-K^2(\omega,\tau)\right]\exp\left[-i\Phi(\omega,\tau)\right]. \quad (2.45)$$

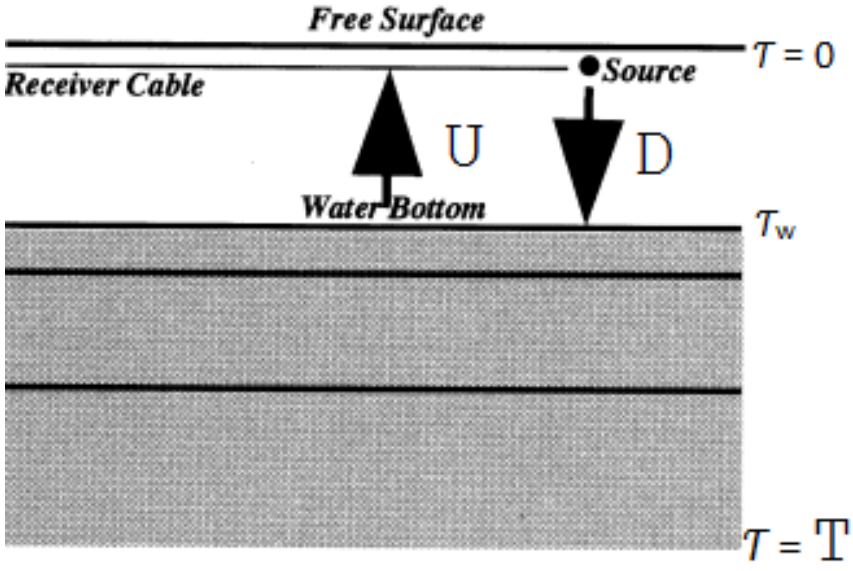

FIGURE 2.1: 1D model: D is the vertically downgoing source wavefield and U is the recorded upcoming wavefield. (Adapted from Yilmaz (2001).)

Figure 2.1 shows 1D stratified earth model whereby T is the maximum thickness of the model in two-way traveltime. As the source is at the top (water) layer, there are no up-going waves at the bottom layer. Therefore, $U(\omega,T) = 0$ when $\tau \geq T$ which implies $K(\omega,T) = 0$. When trying to compute the earth's response $K(\omega,\tau)$ at any depth τ, we can apply the boundary

condition $K(\omega, T) = 0$ up on integration of equation (2.45):

$$-K(\omega,\tau)\exp\big[-i\Phi(\omega,\tau)\big] = -\int_{\tau}^{T} r(\tau')\exp\big[-i\Phi(\omega,\tau')\big]\big[1-K^2(\omega,\tau')\big]\partial\tau'. \tag{2.46}$$

Rearranging equation (2.46) gives

$$K(\omega,\tau) = \exp\big[i\Phi(\omega,\tau)\big]\int_{\tau}^{T} r(\tau')\exp\big[-i\Phi(\omega,\tau')\big]\big[1-K^2(\omega,\tau')\big]\partial\tau', \tag{2.47}$$

where equation (2.47) is now the starting point for a forward and inverse Q modelling algorithms.

With time step $\triangle\tau = 4\times10^{-3}$ seconds, $j\times\triangle\tau$, the integral part of equation (2.47) can be solved using finite difference method:

$$K(\omega,\tau) = \exp\big[i\Phi(\omega,\tau)\big]\bigg[\int_{\tau}^{\tau+\triangle\tau} + \int_{\tau+\triangle\tau}^{\tau+2\triangle\tau} + ... + \int_{(NT-3)\triangle\tau}^{(NT-2)\triangle\tau} + \int_{(NT-2)\triangle\tau}^{(NT-1)\triangle\tau}\bigg]\bigg[\qquad\bigg]\partial\tau', \tag{2.48}$$

by making use of the trapezoid integral

$$\int_{\tau}^{\tau+\triangle\tau} r(\tau')\exp\big[-i\Phi(\omega,\tau')\big]\big[1-K^2(\omega,\tau')\big]\partial\tau' \cong$$

$$\frac{\triangle\tau}{2}\bigg[r(\tau+\triangle\tau)\exp\big[-i\Phi(\omega,\tau+\triangle\tau)\big]\big[1-K^2(\omega,\tau+\triangle\tau)\big]+r(\tau)\exp\big[-i\Phi(\omega,\tau)\big]\big[1-K^2(\omega,\tau)\big]\bigg].$$

Assuming a discretization in τ (sample interval $\triangle\tau$ and total of NT points), calculation of seismogram $K(\omega,\tau)$ in upward direction is done starting at maximum time $T = (NT-1)\triangle\tau$. Introducing the following notation for convenience

$$\begin{aligned}
\tau_j &= j\times\triangle\tau \qquad \& \qquad j = NT-1,\ NT-2,\ ...,\ 0,\\
\omega_l &= 2\pi\times l\times\triangle f \qquad \& \qquad \triangle f = \frac{1}{NT\times\triangle\tau},\\
K^n_{l,j} &= K^n(\omega_l,\tau_j),\\
\chi_{l,j} &= \exp\big[-i\Phi(\omega_l,\tau_j)\big],\\
r_j &= r(\tau_j),
\end{aligned}$$

where the superscript n implies iteration number. The iteration number n represents the number of times a computation cycle repeated, applying each time the previous result, to get successively closer approximations to the solution of equation (2.48). This is because equation (2.48) is non-linear. Therefore, applying the trapezoidal integral in equation (2.48), the $(n+1)^{th}$ iteration is

$$\begin{aligned}
K^{n+1}_{l,j=J} &= \chi^{-1}_{l,j=J}\bigg\{\frac{\triangle\tau}{2}\bigg\}\bigg\{r_J\chi_{l,J}[1-(K^n_{l,J})^2] + 2\sum_{j=NT-2}^{J+1} r_j\chi_{l,j}[1-(K^n_{l,j})^2]\\
&\qquad + r_{NT-1}\chi_{l,NT-1}[1-(K^n_{l,NT-1})^2]\bigg\}, \qquad (2.49)\\
K^n_{l,NT-1} &= K^n(\omega_l,T) = 0, \quad \text{boundary condition.}
\end{aligned}$$

The trapezoid approximation enabled us to calculate the seismogram at each $J = 0, 1, 2, ..., NT - 1$ corresponding to the two-way traveltime $\tau_J = J \times \triangle\tau$ with the seismogram corresponds to the solution $J = 0$, $\tau_0 = 0 \times \triangle\tau = 0$, is at the surface.

So far we have considered the source and receiver are at the surface as is shown in figure 2.1. This works whether the first layer is water or not. Let us consider the source and receiver are deeper in the water layer. Now, we have to take into account surface-related multiples. Figure 2.2 shows water-bottom multiples due to air-water reflection.

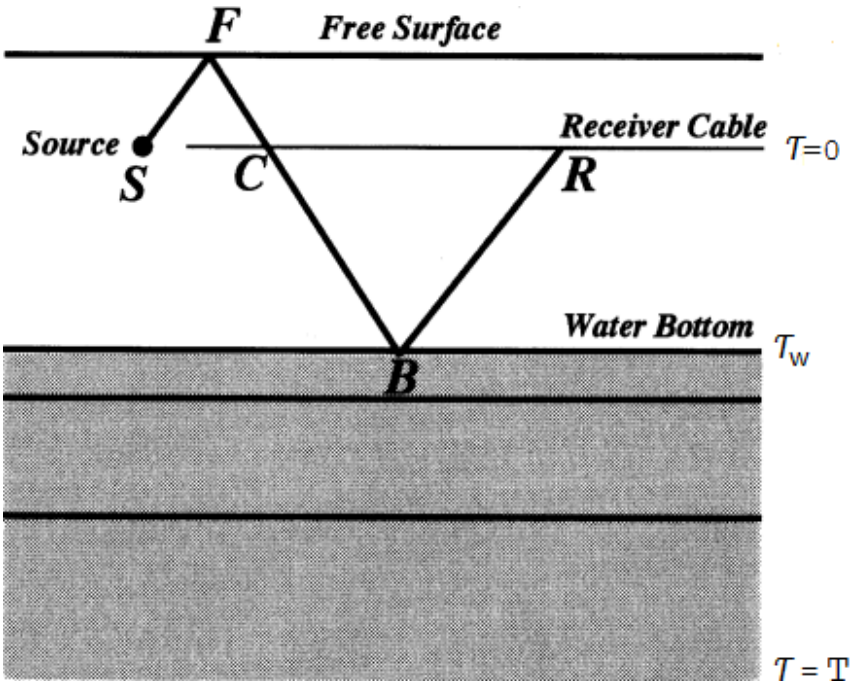

FIGURE 2.2: Water-bottom multiples due to air-water reflection. (Adapted from Yilmaz (2001).)

Assuming that τ_w represents two-way vertical travel time in the water layer, total field $P_l = P(\omega_l)$ recorded at the receiver (including multiples) can then be written as ('R' being the reflection coefficient of the seafloor)

$$\begin{aligned} P_l &= K_{l,j=0}\Big[1 - R\exp(-i\omega_l\tau_w) + R\exp(-2i\omega_l\tau_w) + ...\Big] \\ &= \frac{K_{l,j=0}}{1 + R\exp(-i\omega_l\tau_w)}. \end{aligned} \tag{2.50}$$

The final result in time, the modelled seismogram $k(t, 0)$, is obtained after an inverse fourier transform (FT^{-1}). And for $J = 0$, the matrix representation of

equation (2.49), K^2 being $(K^n)^2$, is as follows:

$$
\begin{bmatrix} K_{0,0}^{n+1} \\ K_{1,0}^{n+1} \\ . \\ . \\ . \\ K_{NT-1,0}^{n+1} \end{bmatrix}
= \frac{\triangle\tau}{2}
\begin{bmatrix}
\left[1-K_{0,0}^2\right] & 2\chi_{0,1}\left[1-K_{0,2}^2\right] & . & 2\chi_{0,NT-2}\left[1-K_{0,NT-2}^2\right] & \chi_{0,NT-1}\left[1-K_{0,NT-1}^2\right] \\
\left[1-K_{1,0}^2\right] & 2\chi_{2,1}\left[1-K_{2,2}^2\right] & . & 2\chi_{1,NT-2}\left[1-K_{1,NT-2}^2\right] & \chi_{1,NT-1}\left[1-K_{1,NT-1}^2\right] \\
. & . & . & . & . \\
. & . & . & . & . \\
. & . & . & . & . \\
\left[1-K_{NT-1,0}^2\right] & 2\chi_{NT,1}\left[1-K_{NT,2}^2\right] & . & 2\chi_{NT-1,NT-2}\left[1-K_{NT-1,NT-2}^2\right] & \chi_{NT-1,NT-1}\left[1-K_{NT-1,NT-1}^2\right]
\end{bmatrix}
\begin{bmatrix} r_0 \\ r_1 \\ . \\ . \\ . \\ r_{NT-2} \\ r_{NT-1} \end{bmatrix}
$$

2.6 Inverse Q Filtering - Non-Linear Case

In the limit $\tau \to 0$ meaning that the receivers are at the surface, equation (2.47) gives the 'seismogram in frequency domain':

$$K(\omega, 0) = \int_0^T r(\tau') \exp\big[-i\Phi(\omega, \tau')\big]\big[1 - K^2(\omega, \tau')\big]\partial\tau'. \tag{2.51}$$

Introducing 'reflectivity' series, specifically 'reflectivity per depth unit series' in this thesis,

$$r(\tau) = \triangle\tau \sum_{j=0}^{NT-1} r_j \delta(\tau - j \times \triangle\tau), \qquad T = (NT-1) \times \triangle\tau, \tag{2.52}$$

equation (2.52) can be written as

$$K(\omega, 0) = \sum_{j=0}^{NT-1} r_j \exp\big[-i\Phi(\omega, j \times \triangle\tau)\big]\big[1 - K^2(\omega, j \times \triangle\tau)\big]\triangle\tau. \tag{2.53}$$

If we drop $K^2(\omega, j \times \triangle\tau)$ of the right hand side of equation (2.53) that is multiples are not included, an expression similar to that of Oliveira & Lupinacci (2013) is achieved which in our case is linear.

Originally, seismogram is recorded in time-domain and sampled with a total of NT samples. Fourier transform of the data will give the same number of monochromatic seismograms and equation (2.53) can be rewritten in a matrix system:

$$\begin{bmatrix} K^{n+1}(0,0) \\ K^{n+1}(1,0) \\ . \\ . \\ . \\ K^{n+1}(NT-1,0) \end{bmatrix} = \tag{2.54}$$

$$\triangle\tau \begin{bmatrix} \chi(0,0)\big[1-(K^n)^2\big] & ... & \chi(0,NT-1)\big[1-(K^n)^2\big] \\ \chi(1,0)\big[1-(K^n)^2\big] & ... & \chi(1,NT-1)\big[1-(K^n)^2\big] \\ . & ... & . \\ . & ... & . \\ . & ... & . \\ \chi(NT-1,0)\big[1-(K^n)^2\big] & ... & \chi(NT-1,NT-1)\big[1-(K^n)^2\big] \end{bmatrix} \begin{bmatrix} r_0^n \\ r_1^n \\ . \\ . \\ . \\ r_{NT-1}^n \end{bmatrix},$$

where

$$\chi_{l,j} = \exp\big[-i\Phi(\omega_l, \tau_j)\big], \qquad \omega_l = 2\pi \times l \times \triangle f \quad \text{and} \quad \tau_j = j \times \triangle\tau.$$

For a given iteration number n, we can compute for the corresponding reflectivity series by solving equation (2.54) employing standard least-squares inversion. Since iteration is repeating a computation cycle applying each time the previous result to get successively closer approximations to the solution, we start by taking $(K^0(\omega))^2 = 0$ for $n = 0$. After a new estimate of the reflectivity series has been obtained, an update of $(K_j^n(\omega))^2$ can be obtained by solving the forward problem in equation (2.49). Iterations are carried out until the relative change in reflectivity is below a certain user set threshold.

To apply least-squares, equation (2.54) can be written in vector and matrix notation in short as

$$\vec{K} = M\vec{r}, \tag{2.55}$$

where

$$\vec{K} = \begin{bmatrix} K^{n+1}(0,0) \\ K^{n+1}(1,0) \\ . \\ . \\ . \\ K^{n+1}(NT-1,0) \end{bmatrix}, \qquad \vec{r} = \begin{bmatrix} r_0^n \\ r_1^n \\ . \\ . \\ . \\ r_{NT-1}^n \end{bmatrix} \quad \text{and}$$

$$M = \triangle\tau \begin{bmatrix} \chi(0,0)\big[1-(K^n)^2\big] & ... & \chi(0,NT-1)\big[1-(K^n)^2\big] \\ \chi(1,0)\big[1-(K^n)^2\big] & ... & \chi(1,NT-1)\big[1-(K^n)^2\big] \\ . & ... & . \\ . & ... & . \\ . & ... & . \\ \chi(NT-1,0)\big[1-(K^n)^2\big] & ... & \chi(NT-1,NT-1)\big[1-(K^n)^2\big] \end{bmatrix},$$

i.e., $\vec{K}$ is a $(N \times 1)$ vector, M is a $(N \times N)$ matrix and $\vec{r}$ is a $(N \times 1)$ vector.

In general, there are more observations than model parameters. Let $\vec{K}$ be the desired seismic output data while the actual output from equation (2.54) is $\vec{S} = M\vec{r}$. We want to compute a reflectivity per depth unit series $\vec{r}$ such that the difference $\vec{\Sigma}$ between the actual output $\vec{S}$ and the predicted seismic output data $\vec{K}$ is minimum in the least-squares sense. Therefore, the error $\vec{\Sigma}$ with respect to parameter vector $\vec{r}$ is

$$\vec{\Sigma} = \vec{K} - \vec{S} = \vec{K} - M\vec{r}. \tag{2.56}$$

And the cumulative squared error,

$$\begin{aligned}\vec{\Sigma}^{T*}\vec{\Sigma} &= (\vec{K}-M\vec{r})^{T*}(\vec{K}-M\vec{r}),\\ &= \vec{K}^{T*}\vec{K}-\vec{K}^{T*}M\vec{r}-\vec{r}^{T*}M^{T*}\vec{K}+\vec{r}^{T*}M^{T*}M\vec{r},\end{aligned} \tag{2.57}$$

where T denotes matrix transpose and $*$ denotes complex conjugate.

We want to estimate a reflectivity per depth unit series $\vec{r}$ such that the quantity $\vec{\Sigma}^{T*}\vec{\Sigma}$ is minimum. This condition leads to setting the derivative of $\vec{\Sigma}^{T*}\vec{\Sigma}$ with respect to $\vec{r}$ to zero. Differentiate both sides of equation (2.57) with respect to $\vec{r}$ and observe the requirement for least-squares procedure minimization that

$$\frac{\partial\vec{\Sigma}^{T*}\vec{\Sigma}}{\partial\vec{r}} = -\vec{K}^{T*}M+\vec{r}^{T*}M^{T*}M=0. \tag{2.58}$$

Because $\vec{r}^{T*}$ is complex valued, $\partial\vec{r}^{T*}/\partial\vec{r}=0$. Thus, applying matrix transpose and rearranging the terms of equation (2.58)

$$\begin{aligned}(M^{T*}M)^{T*}\vec{r} &= M^{T*}\vec{K} \quad\Longrightarrow\quad (M^{T*}M)\vec{r}=M^{T*}\vec{K},\\ \Longrightarrow\vec{r} &= (M^{T*}M)^{-1}M^{T*}\vec{K}.\end{aligned} \tag{2.59}$$

Subsequently, it is also possible to compute the acoustic impedance $AI(\tau)=\rho(\tau)v_r(\tau)$. Following equation (2.36)

$$r(\tau)=\frac{1}{2\rho v_r}\frac{\partial(\rho v_r)}{\partial\tau},\Longrightarrow\rho(\tau)v_r(\tau)=\rho(0)v_r(0)\exp\left[2\int_0^\tau r(\tau')d\tau'\right],$$

and applying equation (2.47), the acoustic impedance $AI_j=\rho(\tau_j)v_r(\tau_j)$ at τ_j from the surface can be put as

$$AI_j=AI_0\exp\left[2\triangle\tau\sum_{i=0}^{j}r_j\right]\quad\text{for}\quad j=0,1,2,...,NT-1. \tag{2.60}$$

AI_0 is easily known since the first layer is sea water in marine seismic.

Finally we can compute the reflectivity series R_j as in

$$R_j=\frac{AI_{j+1}-AI_j}{AI_{j+1}+AI_j}=\frac{\exp\left[2\triangle\tau r_{j+1}\right]-1}{\exp\left[2\triangle\tau r_{j+1}\right]+1}\quad\text{for}\quad j=0,1,2,...,NT-1. \tag{2.61}$$

This will enable us to compare and contrast our results with other inversion methods as many of those inversion methods compute reflectivity series. Indeed, both the reflectivity series R_j and reflectivity per unit depth r_j (in this thesis work) show acoustic impedance contrast. But they differ both in magnitude and dimensionality.

In the next two chapters we will implement the developed model in Matlab by specifying layered model parameters, generate synthetic seismogram using the forward model, and perform inversion taking the forward modelled synthetic seismogram as an input.

Chapter 3

Forward Q Simulation - Matlab

Layered implementation of forward Q modelling is considered. For Q compensation, generally, we only require absorptive information for major layers. In this approach, the earth model is assumed to be a one-dimensional (1-D) function varying with depth in two-way traveltime.

3.1 Model Parameters

In order to perform forward Q simulation, first a stratified earth model with N number of layers is specified, the first layered being sea water in marine seismic. For each layer, thickness z_j $[m]$, velocity v_j $[m/s]$, density ρ_j $[g/cm^3]$ and quality factor Q_j $[dimensionless]$ are assigned as is shown in table 3.1. The corresponding Matlab generated model is shown in figure 3.1.

Layer	thickness z $[m]$	density ρ $[g/cm^3]$	velocity v $[m/s]$	quality factor Q $[dimensionless]$
1^{st}	200	1.0	1500	20
2^{nd}	300	1.5	2000	25
3^{rd}	400	1.7	2500	30
4^{th}	500	2.2	3000	35

TABLE 3.1: Input model parameters of a four layer earth model.

The acoustic impedance AI_j $[(m/s).(g/cm^3)]$ of each layer is computed, the product of velocity and density, i.e.,

$$AI_j = v_j \rho_j, \qquad j = 1, ..., N. \tag{3.1}$$

While the reflectivity series R_j $[dimensionless]$ can be calculated as

$$R_j = \frac{v_{j+1}\rho_{j+1} - v_j \rho_j}{v_{j+1}\rho_{j+1} + v_j \rho_j}, \qquad j = 1, ..., N-1. \tag{3.2}$$

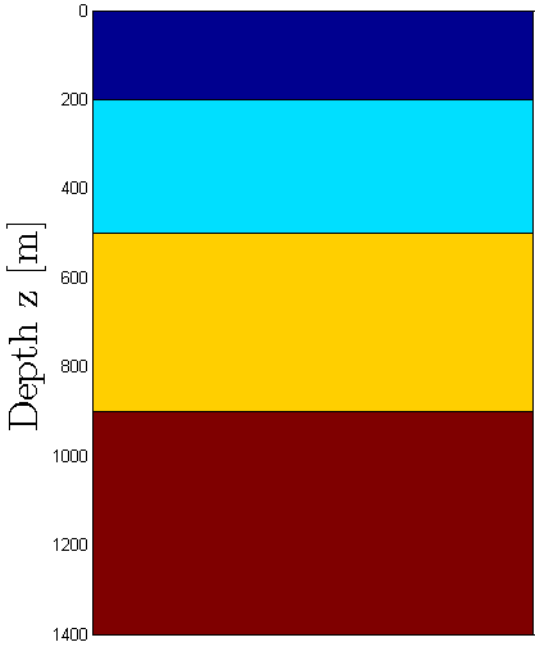

FIGURE 3.1: 1D-Earth model with four layers.

The next step is converting the layer thickness z_j $[m]$ into two-way traveltime τ_j $[s]$ which can be calculated as follows:

$$\tau_j = 2\frac{z_j}{v_j}, \qquad j = 1, ..., N. \tag{3.3}$$

Then the total thickness of the model in two-way traveltime T_M $[s]$ is

$$T_M = \sum_{j=1}^{N} \tau_j = 2\sum_{j=1}^{N} \frac{z_j}{v_j}. \tag{3.4}$$

Once we have computed the total model thickness T_M in two-way traveltime, the next step is to sample the physical parameters: layer acoustic impedance AI, reflectivity series R and quality factor Q, in sampling time say $\triangle\tau = 0.004\,s$ and NT samples. Therefore, from the ratio of subsequent sampled acoustic impedance $AI_j = AI(\tau_j)$, the reflectivity per depth unit series r_j $[1/s]$ is computed as in:

$$r(\tau_j) = r_j = \frac{1}{2\triangle\tau}\left[\frac{v_{j+1}\rho_{j+1}}{v_j\rho_j} - 1\right], \qquad j = 1, ..., NT-1, \tag{3.5}$$

where $\triangle\tau = \tau_{j+1} - \tau_j$. It is clear from equations (3.2) and (3.5) that the reflectivity R_j and the reflectivity per depth unit series r_j are two similar physical parameters which represent the contrast in acoustic impedance across an interface. The main difference is their dimensionality.

The sampled acoustic impedance AI_j of the generated model of table 3.1 is shown in figure 3.2. It is evident from figure 3.2 that the acoustic impedance is

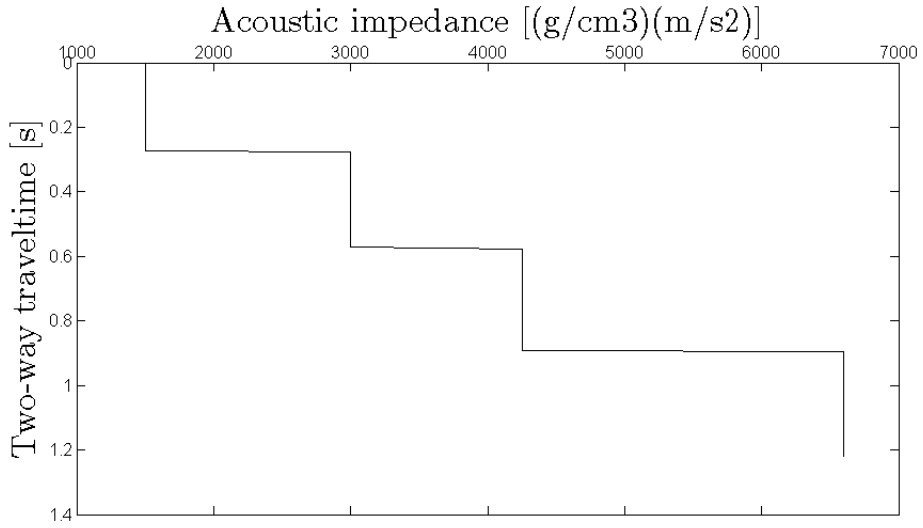

FIGURE 3.2: Acoustic impedance AI of a four layer earth model.

blocked (constant) over a certain range in depth. This is because both velocity and density are assumed constant over a certain layer. Similarly, the sampled quality factor is blocked (constant) over a certain range in depth as is shown in figure 3.3.

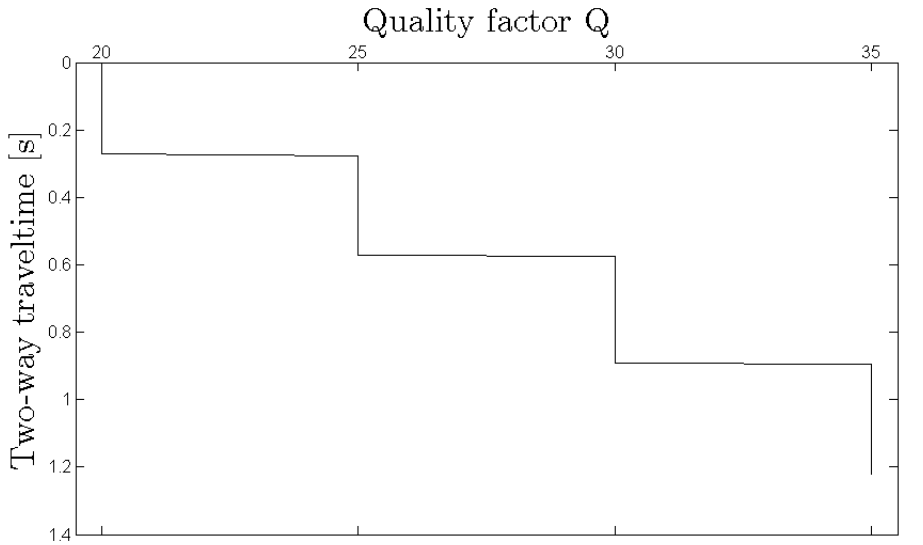

FIGURE 3.3: Quality factor (QF) of a four layer earth model.

Since the number of interfaces in this case are three, ignoring of course air-sea surface interface, it can be seen from figures 3.4 and 3.5 that there are three non-zero values of reflectivity series R and reflectivity per depth unit series $r(\tau)$ corresponding to those three interfaces.

In order to get the synthetic seismogram $k(t, \tau)$ in time domain by inverse Fourier transform of the complex reflection coefficient (approximately) $K^{n+1}_{l,j=J}$ derived in equation (2.49), each component of $K_{l,j}$ is multiplied by a sampled

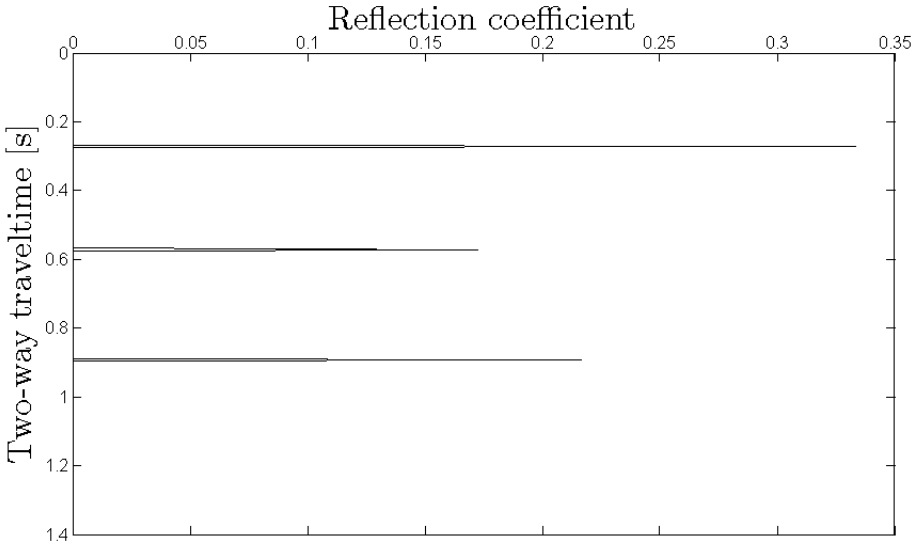

FIGURE 3.4: Reflectivity series R of a four layer earth model.

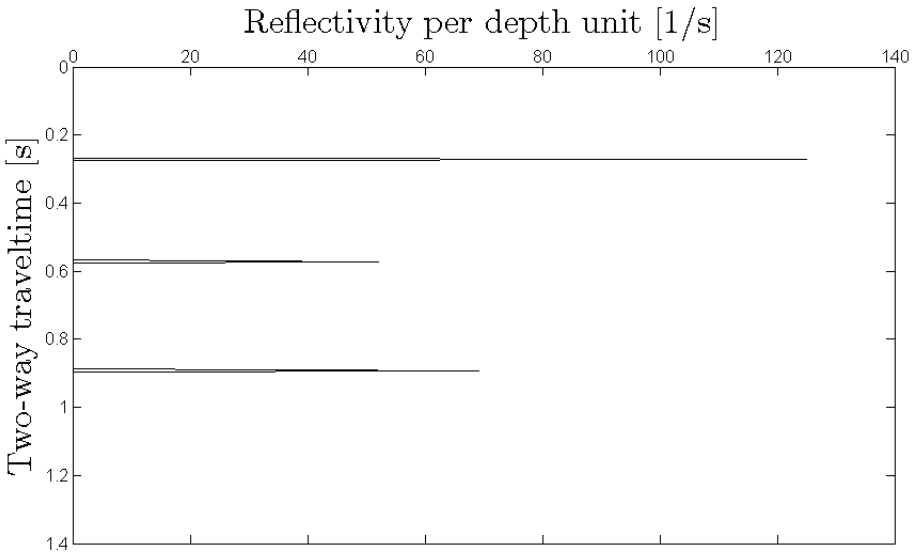

FIGURE 3.5: Reflectivity per depth unit series $r(\tau)$ of a four layer earth model.

Ricket-wavelet in frequency domain:

$$\begin{aligned} srw &= \frac{2}{\sqrt{\pi}} \times \frac{f^2}{f_c^3} \times \exp\left[-\frac{f}{f_c}\right]^2, \\ & f = l \times \triangle f \quad \text{and} \quad l = 0, 1, 2, ..., NT, \end{aligned} \tag{3.6}$$

with the center frequency f_c being chosen to be $20\,Hz$ in this thesis. This Ricker-wavelet is a zero-phase wavelet and non-causal. It is often used as a zero-phase embedded wavelet in modelling and synthetic seismogram manufacture.

3.2 Seismogram $k(t,0)$ and Absorption $Y(\omega,\tau_j)$

The magnitude and shape of the seismogram $k(t,0)$ computed by forward Q simulation depend on the absorption function $Y(\omega,\tau)$, with $Y(\omega,\tau)=1$ being absorption free. It is useful to understand in general how the amplitude attenuation and wavelet broadening effects are related to the real and imaginary parts of the absorption function $Y(\omega,\tau)=A(\omega,\tau)+iB(\omega,\tau)$. The imaginary part is mainly associated with amplitude attenuation whereby $B(\omega,\tau)\longrightarrow 0$ leads to higher amplitude of the seismic seismogram $k(t,0)$. Similarly the real part is mainly related with broadening of seismic seismogram $k(t,0)$ whereby $A(\omega,\tau)\longrightarrow 1$ results in less broadening. It is shown in equation (2.15) of chapter 2 how $A(\omega,\tau)$ and $B(\omega,\tau)$ are related to the quality factor Q of the medium depending on the Q-model chosen. Therefore, the absorption function of Wang & Guo (2004*a*) Q-model sampled in time and frequency becomes:

$$\begin{aligned}\frac{1}{\sqrt{Y_{Wang}(l,j)}} &\approx \left[\frac{f_h}{l\times\triangle f}\right]^{\gamma_j}\left[1-i\frac{1}{2Q_j}\right], \qquad (3.7)\\ f_h &\equiv \text{highest frequency (125 Hz in this thesis)},\\ \gamma_j &= [\pi Q_j]^{-1},\\ l &= 0,1,2,...,NT-1 \quad \& \quad j=0,1,2,...,NT-1.\end{aligned}$$

Similarly, the absorption function of the alternative Futterman (1962) Q-model is sampled both in time and frequency, and is slightly modified as:

$$\begin{aligned}\frac{1}{\sqrt{Y_{Futt}(l,j)}} &\approx \left[1+\frac{1}{l\times\triangle f}\aleph_{l,j}\right]^{-1}-i\frac{1}{2Q_j}, \qquad (3.8)\\ \aleph_{l,j} &= \aleph\left(\frac{l\times\triangle f}{2Q_j}\right) \quad \text{Hilbert transform},\\ l &= 0,1,2,...,NT-1 \quad \& \quad j=0,1,2,...,NT-1.\end{aligned}$$

Finally, the case $v(\omega)=v_r$ implies no dispersion, the corresponding absorption function is sampled only in time and becomes

$$\frac{1}{\sqrt{Y_{no-disp}(j)}}\approx 1-i\frac{1}{2Q_j}, \quad \text{where} \quad j=1,2,...,NT. \qquad (3.9)$$

If the quality factor is extremely large, $Q\rightarrow\infty$, then $(1/Q)\rightarrow 0$. Hence, all the mentioned Q-models become absorption free, that is $Y(\omega,\tau)\simeq 1$. In

	z $[m]$	ρ $[g/cm^3]$	v $[m/s]$	$A(\omega,\tau)+iB(\omega,\tau)$	
Layer 1	200	1.0	1500	1+i0	Absorption
Layer 2	300	1.5	2000	1+i0	free

TABLE 3.2: Two layer model parameters assumed.

a practical sense the absorption free $Y(\omega, \tau) \simeq 1$ correspond to a large finite Q-value beyond which there is almost no absorption. To observe attenuation and dispersion effects, first an absorption free seismogram $k(t, 0)$, is generated using a very simple two layer model (table 3.2). The seismogram, which here only a single reflection, is shown in figure 3.6.

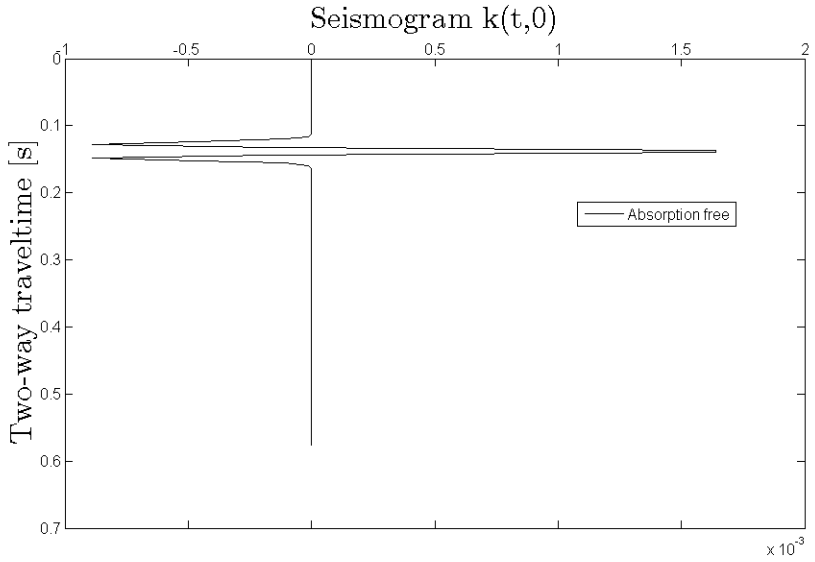

FIGURE 3.6: Forward modelled absorption free seismogram, k(t,0).

Now using Wang & Guo (2004*a*) Q-model, a seismogram $k(t, 0)$ is generated corresponding to different Q-values say Q = 400, 200, 100, 50 and 25. These set of Q-values are used by Wang (2008) and Montaña & Margrave (2004) to study attenuation hence enabled us to draw comparisons.

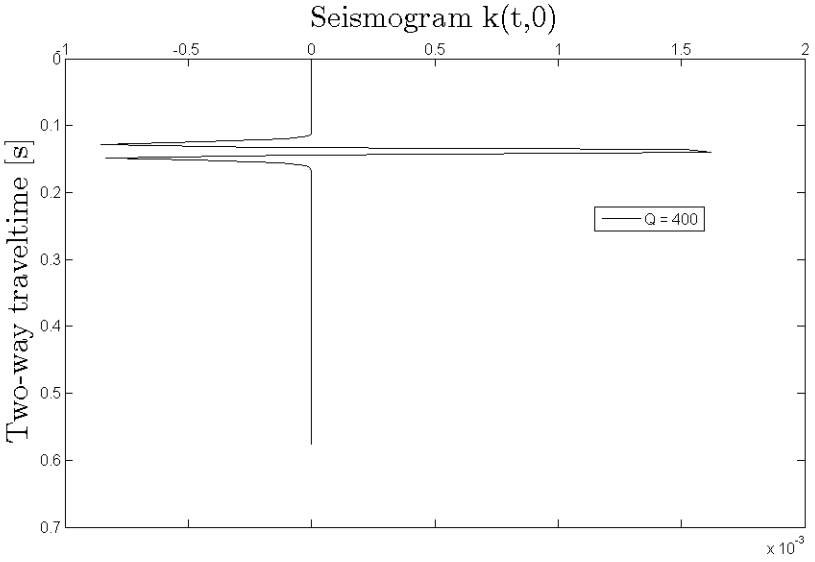

FIGURE 3.7: Forward modelled seismogram, k(t,0) using Q = 400.

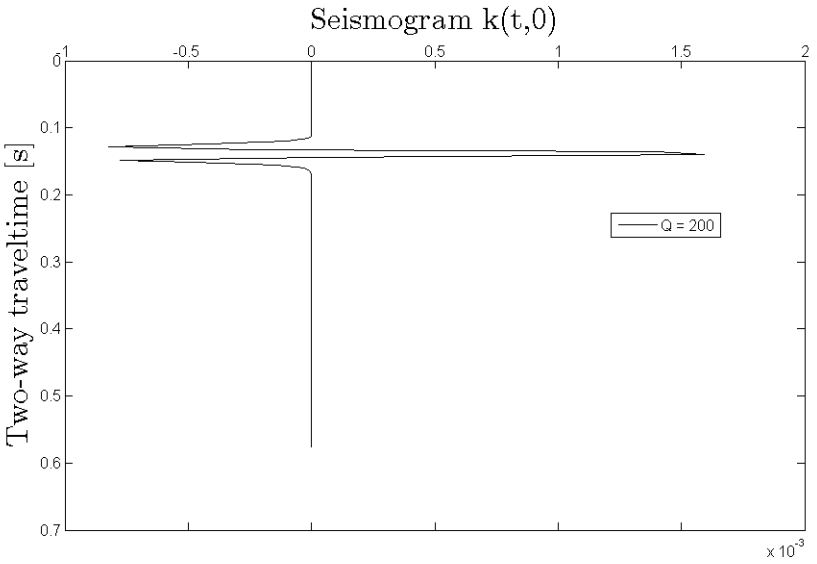

FIGURE 3.8: Forward modelled seismogram, k(t,0) using Q = 200.

Figures 3.6 - 3.11 show that the amplitude and shape of the seismogram $k(t,0)$ change with the quality factor Q. As the quality factor Q gets smaller, the absorption coefficient $\alpha \propto 1/Q$ increases, the amplitude of the seismogram $k(t,0)$ decreases accompanied by broadening. Though we are dealing with zero offset in this thesis, nonetheless for two layer model similar result is shown in Cheng & Margrave (2011). Moreover, figures 3.6 and 3.7 show that the quality factor $Q = 400$ is the threshold value beyond which we do not observe absorption with our model setup. Similar result is shown in Wang (2008).

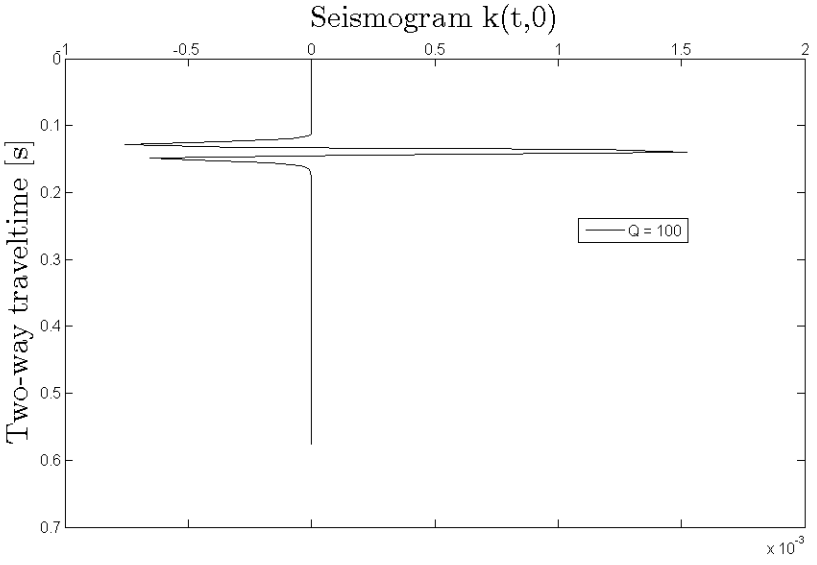

FIGURE 3.9: Forward modelled seismogram, k(t,0) using Q = 100.

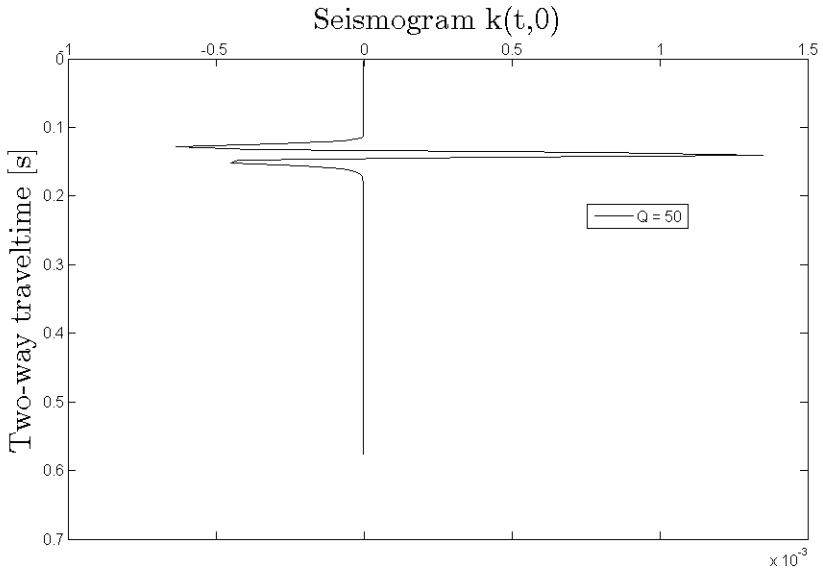

FIGURE 3.10: Forward modelled seismogram, k(t,0) using Q = 50.

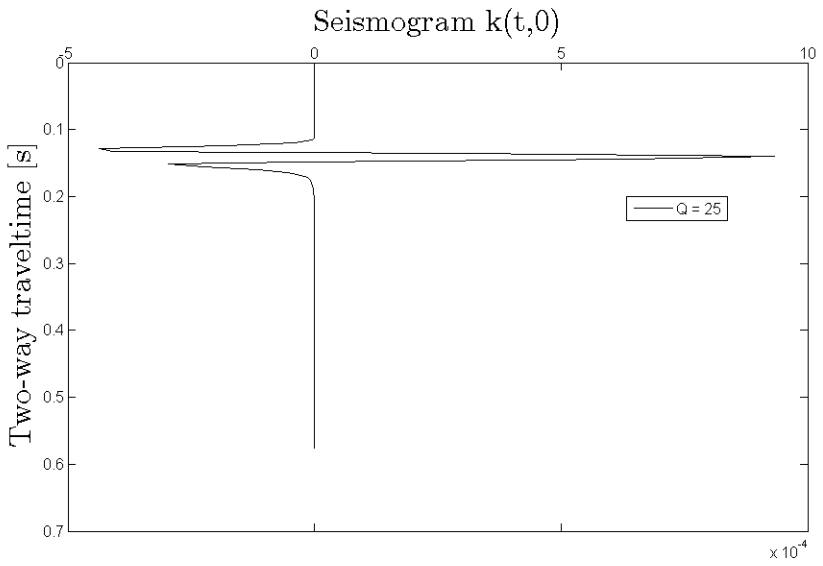

FIGURE 3.11: Forward modelled seismogram, k(t,0) using Q = 25.

3.3 Synthetic Seismogram without Multiples

By dropping the K^2 in right-hand-side of equation (2.49), a linear-forward wave propagation model is obtained,

$$K_{l,j=J} = \chi^{-1}_{l,j=J}\left\{\frac{\triangle\tau}{2}\right\}\left\{r_J\chi_{l,J} + 2\sum_{j=NT-2}^{J+1} r_j\chi_{l,j} + r_{NT-1}\chi_{l,NT-1}\right\}. \tag{3.10}$$

Equation (3.10) is similar to the downward wave propagation model discussed by Montaña & Margrave (2004), Wang (2006), van der Baan (2012). To get

the corresponding synthetic seismogram $k(t,0)$ using Wang & Guo (2004*a*) Q-model, the following four layer model parameters specified in table (3.3) are used. The resulting synthetic seismogram $k(t,0)$ without multiples, is shown in

Layer	thickness z $[m]$	density ρ $[g/cm^3]$	velocity v $[m/s]$	quality factor Q $[dimensionless]$
1^{st}	200	1.0	1500	20
2^{nd}	300	1.5	2000	25
3^{rd}	400	1.7	2500	30
4^{th}	500	2.2	3000	35

TABLE 3.3: Input model parameters of a four layer earth model.

figure 3.12. Similar result has been found using alternative Futterman (1962)

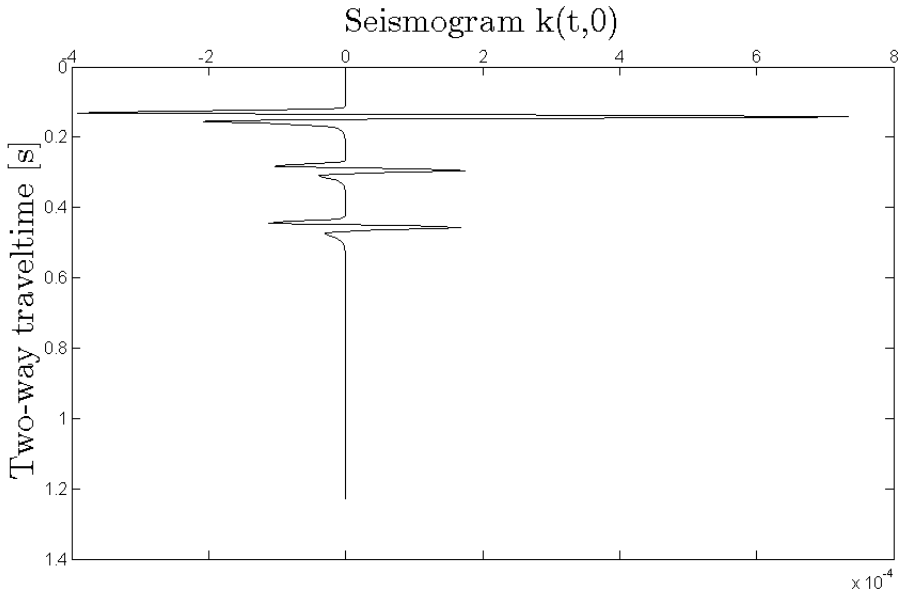

FIGURE 3.12: Synthetic seismogram $k(t,0)$ without any multiples using Wang's modified Kolsky Q model.

Q-model of equation (3.8) is shown in figure 3.13. No major difference is observed in synthetic seismogram $k(t,0)$ for the two Q-models. And to complete the discussion, figure 3.14 shows the dispersion free non-causal seismogram generated by using equation (3.9).

3.4 Synthetic Seismogram with Multiples

Full solution, that is equation (2.49), is applied in order to include the multiples. Yet, the surface-related water-bottom multiples due to water-air interface are not included. Using the dispersionless Q-model of equation (3.9) the

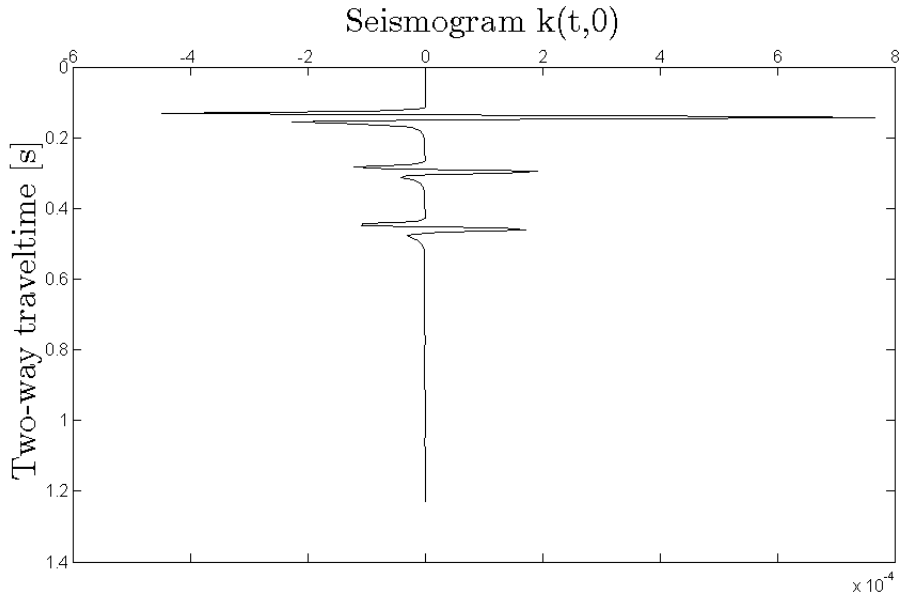

FIGURE 3.13: Synthetic seismogram $k(t,0)$ without any multiples using causal Futterman (1962) Q model.

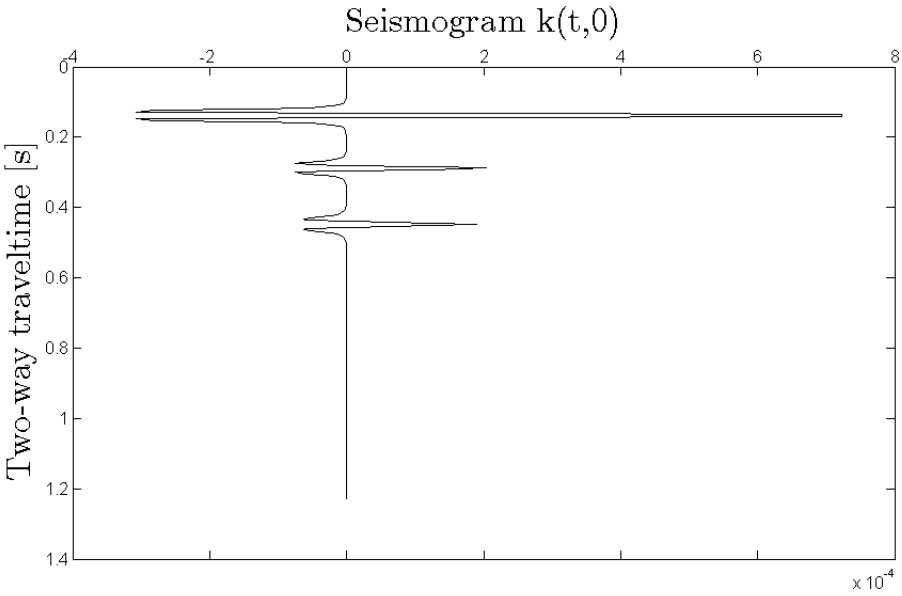

FIGURE 3.14: Synthetic seismogram $k(t,0)$ without any multiples using non-causal Futterman (1962) Q model.

synthetic seismogram $k(t,0)$ without the surface-related multiples is shown in figure 3.15. The multiples can be seen, though they are smaller, than the main reflections.

Once again in order to include the surface-related water-bottom multiples the solution given in equation (2.50) is applied. Correspondingly the synthetic seismogram $k(t,0)$ using the dispersionless Q-model of equation (3.9) including

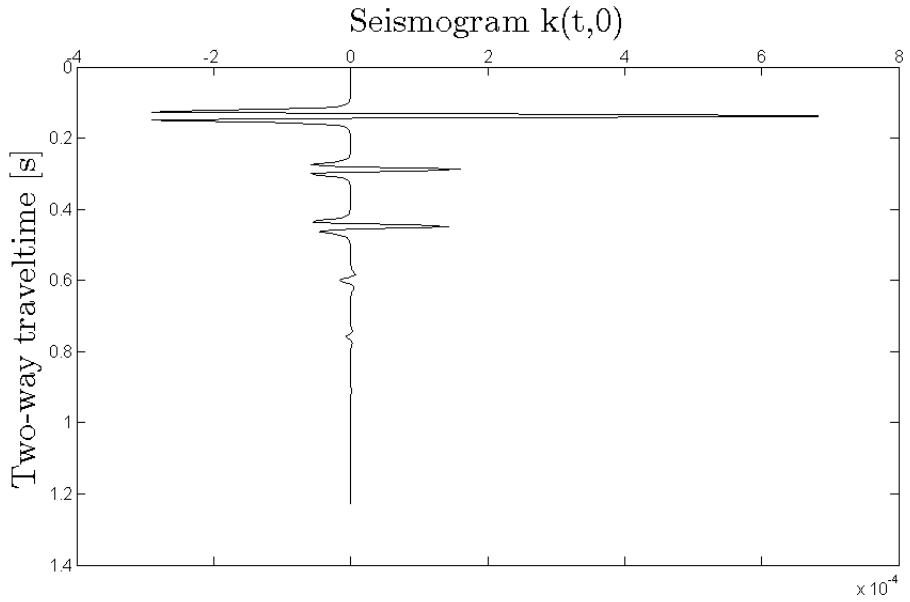

FIGURE 3.15: Synthetic seismogram $k(t, 0)$ without free-surface multiples, after 8 iterations.

the free-surface multiples is shown in figure 3.16. It can be seen that the water-bottom multiples have opposite polarity than the main reflections.

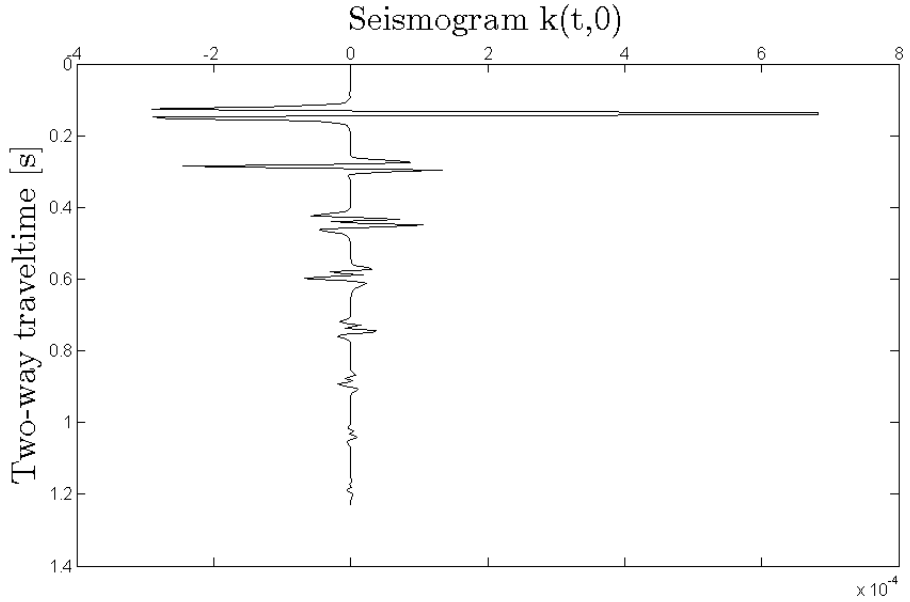

FIGURE 3.16: Synthetic seismogram $k(t, 0)$ including the free-surface multiples, after 8 iterations.

Chapter 4

Inversion - Matlab

The inversion procedure is formulated on the basis that the seismogram at the surface $K(\omega, 0)$ is a known quantity, while the reflectivity per depth unit series $r(\tau)$ is the unknown which is to be determined. This seismogram $K(\omega, 0)$ can be field or synthetic seismic data.

So far, in forward Q modelling, the reflectivity per depth unit series $r(\tau)$ is known from the input layered model parameters. It provides the computation of synthetic seismogram $k(t, 0)$ using Futterman (1962) and Wang & Guo (2004*a*) Q-models. By using the forward modelled synthetic seismogram $K(\omega, 0)$ as an input, inversion is performed to compute the reflectivity per depth unit series $r(\tau)$ thereby calculate the acoustic impedance of the structure understudy. To do so, an algorithm of equation (2.59) is developed in Matlab.

It worth to mention that while modelling of absorption effects of sediment-layers (reservoir), the quality factor Q-values often used are ranging from around 20 up to 200, (Klimentos 1995, Mitchell & Hwang 1987, Oliveira & Lupinacci 2013, Robinson 1979, Wang & Guo 2004*b*). This range is inline with the assumption 'small to moderate absorption' made in chapter 2, (Futterman 1962).

4.1 Inversion Using Same Q-value

In this first section, we use same Q-values to calculate synthetic seismogram $\vec{K}$ and the matrix M used to perform the inversion to get the reflectivity per depth unit series $\vec{r}$. To avoid aliasing lower frequencies are used during the inversion process. Moreover, due to the singularity of the generated matrix $M^{T*}M$, a suitable damping constant λ is introduced in calculating the $(M^{T*}M)^{-1}$ of equation (2.59). This suitable damping constant λ is chosen out from the singular value decomposition (svd) of $M^{T*}M$, thus transform the matrix $M^{T*}M$ into invertible new matrix:

$$\vec{L} = svd(M^{T*}M) \quad \Longrightarrow \quad M^{T*}M + \lambda I, \tag{4.1}$$

where I a unitary matrix of the same order as matrix $M^{T*}M$. The suitable damping constant λ is found around the $(NT/2)^{th}$ eigenvalue of $M^{T*}M$ in this thesis. Moreover, if we drop K^2 in computing M of equation (2.55), we have linear inversion. That is multiples are not included.

Let us start with the input model parameters given in table (4.1). The corresponding reflectivity per depth unit $r(\tau)$ shown in figures 4.1 which is independent of the three sets of quality factor Q-values. Applying forward Q modelling, we have seen in chapter 3, we can compute the synthetic seismogram $K(\omega, 0)$ using these specified model parameters. It is worth to mention that the synthetic seismogram $K(\omega, 0)$ is complex-valued though the specified input parameters reflectivity per depth unit $r(\tau)$ and quality factor Q are real-valued.

Layer	thickness	density	velocity	quality factor		
	z $[m]$	ρ $[g/cm^3]$	v $[m/s]$	Q_1	Q_2	Q_3
1^{st}	200	1.0	1500	20	105	∞
2^{nd}	300	1.5	2000	25	100	∞
3^{rd}	400	1.7	2500	30	115	∞
4^{th}	500	2.2	3000	35	110	∞

TABLE 4.1: Input model parameters of a four layer earth model.

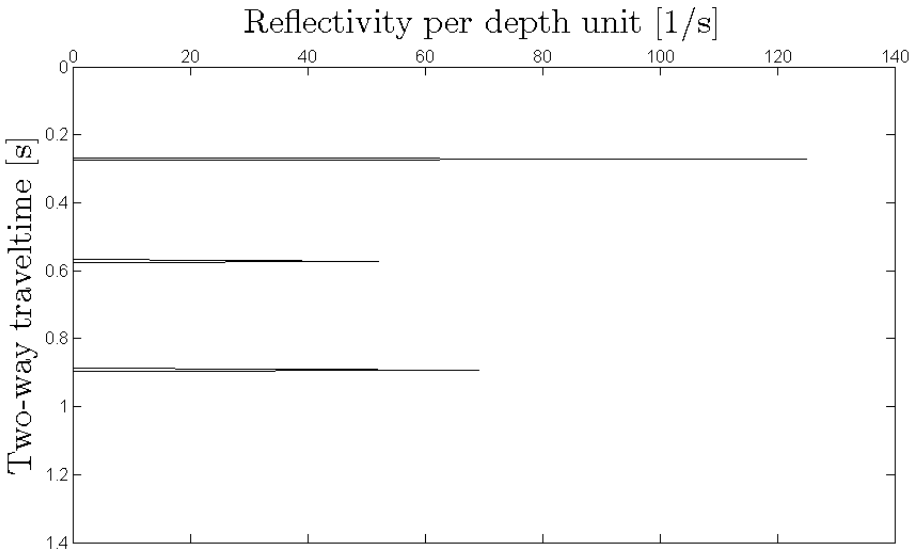

FIGURE 4.1: Reflectivity per depth unit series $r(\tau)$ of a four layer earth model.

Now using the quality factor set Q_1-values given in table (4.1), we have computed the matrix M of equation (2.55) and input synthetic seismogram $K(\omega, 0)$. Inversion is performed using same set Q_1-values. And, we have repeated this process for sets Q_2- and Q_3-values. By doing so, in principle,

we should get the same reflectivity per depth unit $r(\tau)$ series as is shown in figure 4.1 which is real-valued as the input layer acoustic impedance and velocity are real-valued. Instead, what is found by computing equation (2.59) is complex-valued with the real part shown in figures 4.2 and 4.3 corresponding to linear (without multiples) and non-linear (with multiples assuming iteration $n = 8$) inversion cases respectively. There is still no dependence on value of the quality factor used. The decrease in amplitude is in part attributed to the damping constant λ introduced due to the singularity the matrix $M^{T*}M$.

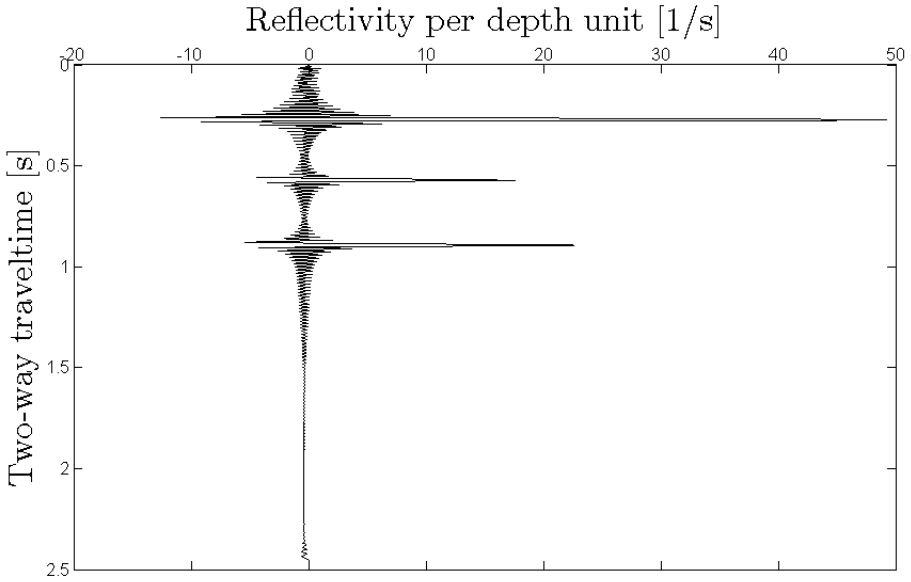

FIGURE 4.2: Inversion using the same Q, linear case.

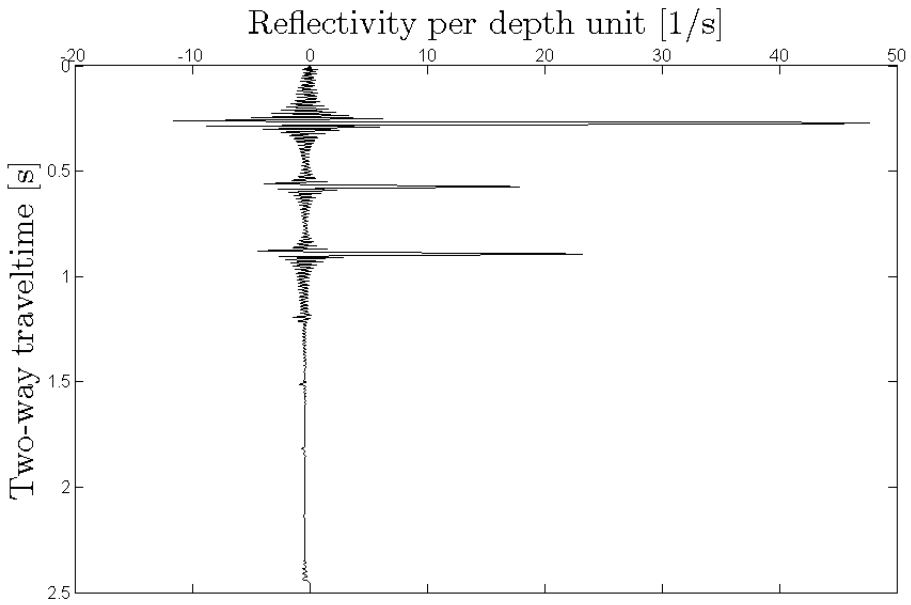

FIGURE 4.3: Inversion using the same Q, non-linear case after 8 iterations.

To eliminate the noise that appears in figures 4.2 and 4.3, a second order butterworth low pass band-filter with cut-off frequency of $\frac{NT}{3} f_{Nqst}$ is used, where NT is the total number of samples and f_{Nqst} is Nyquist frequency. It resulted in a better resolution of the reflectivity per depth unit series $r(\tau)$ shown in figures 4.4 and 4.5. As can be seen in figures 4.5, though smaller, the multiples appear.

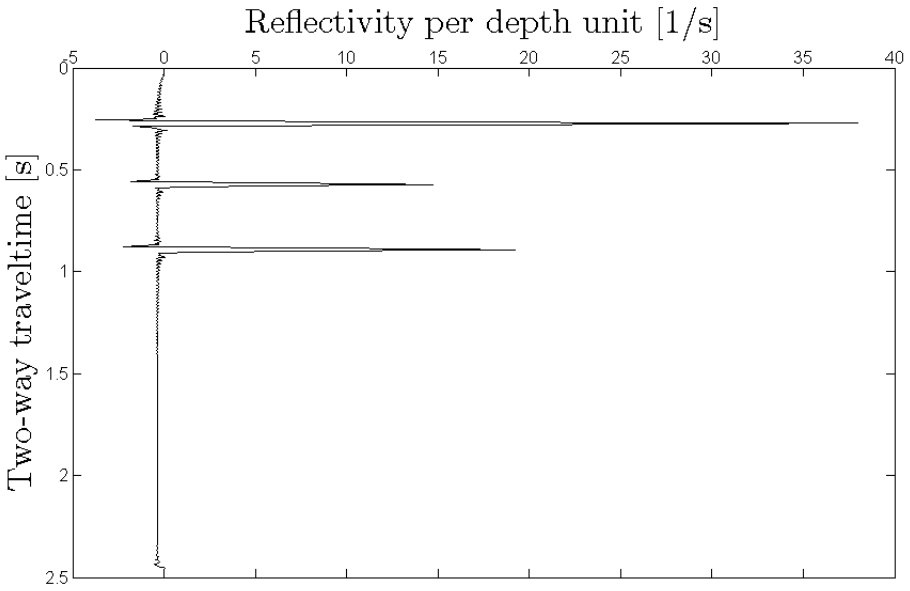

FIGURE 4.4: Inversion using the same Q plus band-pass, linear case.

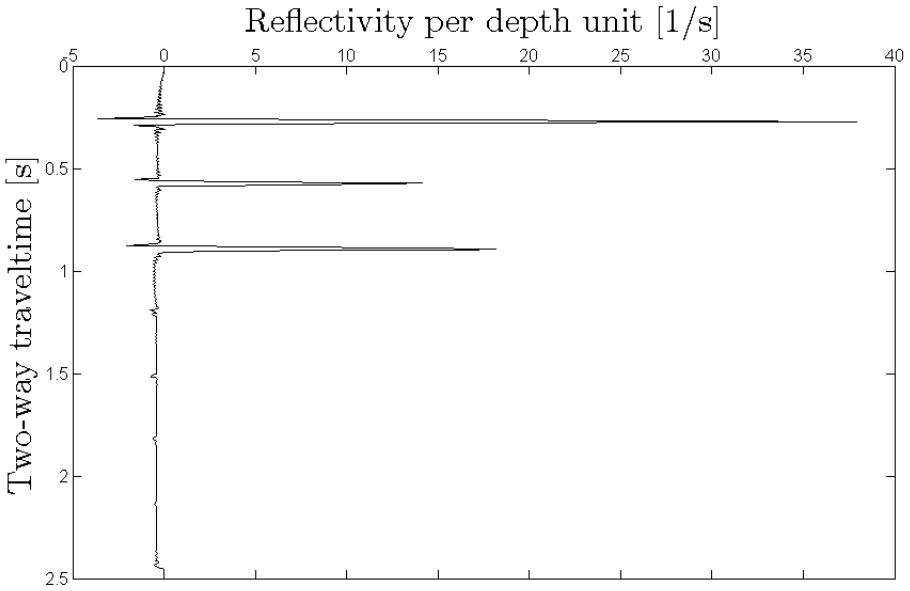

FIGURE 4.5: Inversion using the same Q plus band-pass, non-linear case after 8 iterations.

For comparison purposes with other inversion models, the reflectivity series

$R(\tau)$ shown in figure 4.6 is computed using equation 2.61 from the reflectivity per depth unit $r(\tau)$ shown in figure 4.5 above. As it should, $\mid R(\tau) \mid < 1$ unlike that of $r(\tau)$.

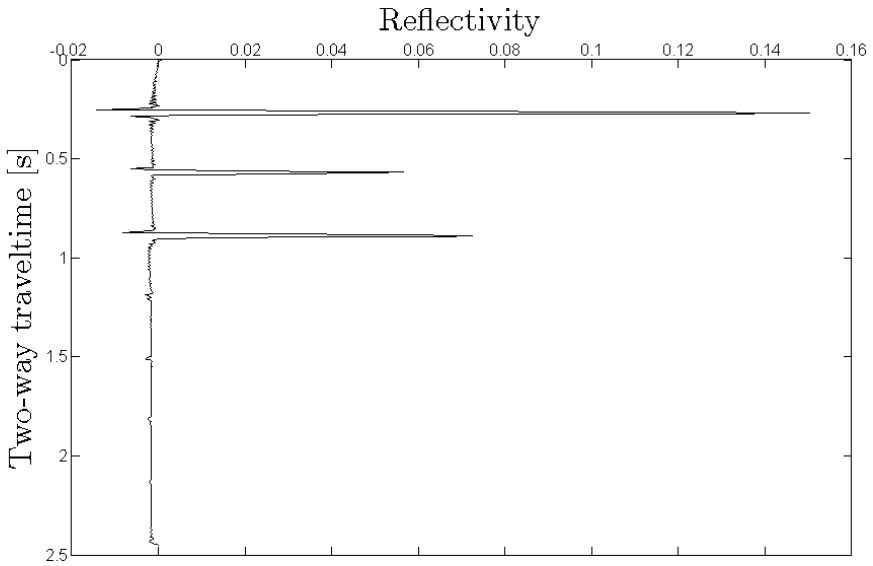

FIGURE 4.6: Reflectivity series $R(\tau)$, non-linear case after 8 iterations.

Moreover, if we can compute the acoustic impedance of the first layer then the acoustic impedance of the subsurface understudy can be computed using equation 2.60. Assuming the first layer being sea water in our model and using the reflectivity per depth unit $r(\tau)$ shown in figure 4.5, the acoustic impedance via inversion and forward modelled are shown in figure 4.7. The computed acoustic impedance $AI(\tau)$ via inversion is complex-valued, with the real part plotted in figure 4.7.

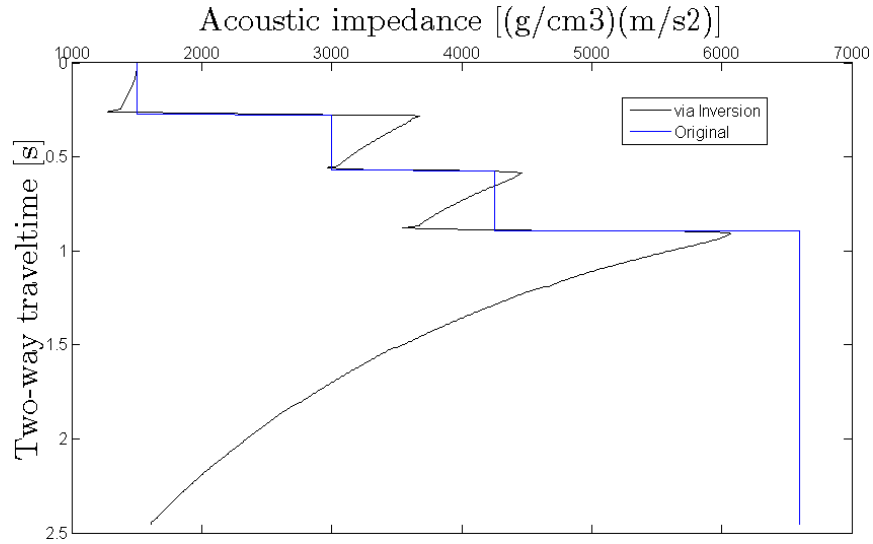

FIGURE 4.7: Acoustic impedance $AI(\tau)$, non-linear case after 8 iterations.

To avoid aliasing lower frequencies are used during the inversion process with the highest frequency being $\frac{NT}{2} f_{Nqst}$. Now let us change the cut off frequency of the second order butterworth low pass filter from $\frac{NT}{3} f_{Nqst}$ to $\frac{2NT}{5} f_{Nqst}$ and $\frac{NT}{2} f_{Nqst}$, the reflectivity per depth unit shown in figure 4.3 become figures 4.8 and 4.9 respectively. As it should be there is no significant difference between figure 4.3 and 4.9 as the cut off frequency of the second order butterworth low pass considered is same as the the highest frequency $\frac{NT}{2} f_{Nqst}$ used in the inversion process.

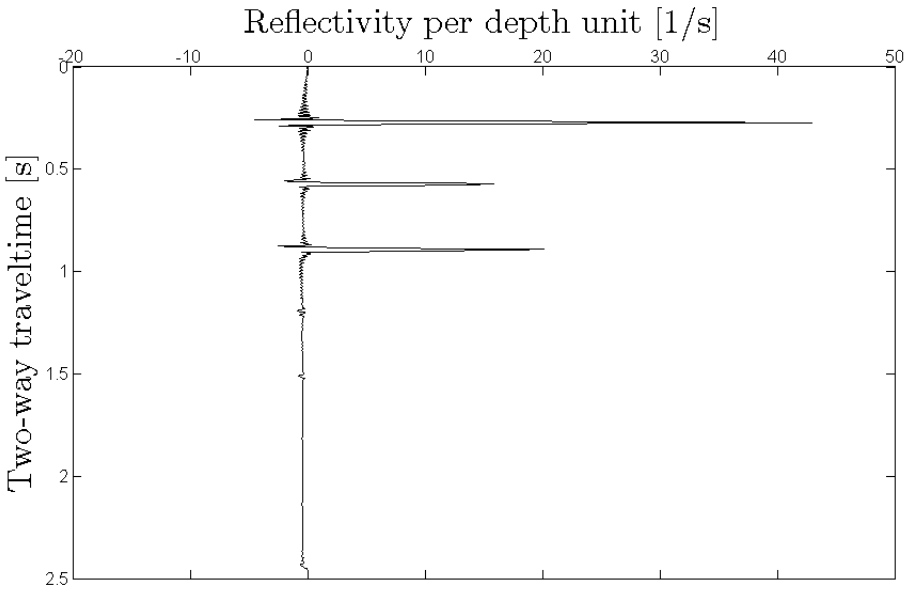

FIGURE 4.8: Inversion using the same Q, non-linear case after 8 iterations.

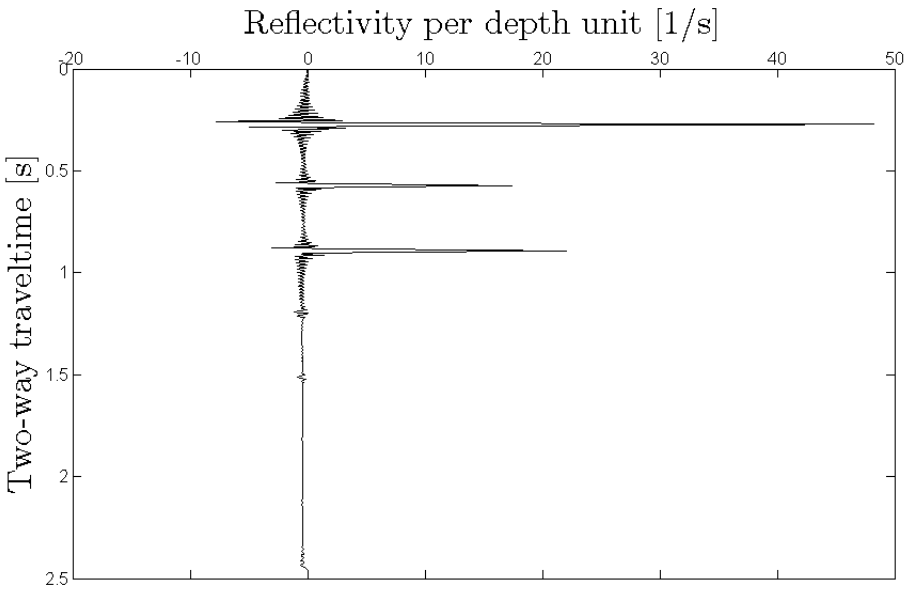

FIGURE 4.9: Inversion using the same Q, non-linear case after 8 iterations.

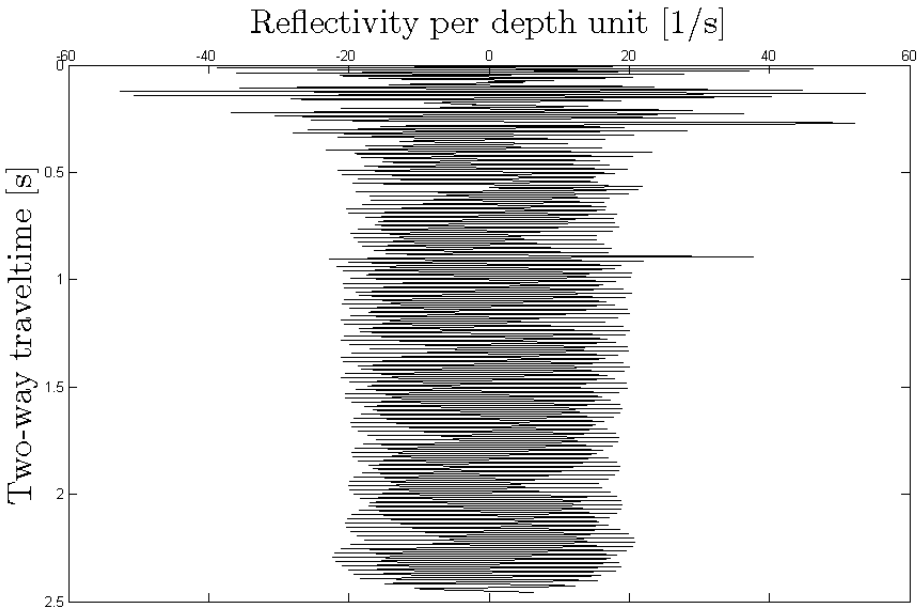

FIGURE 4.10: Inversion, damping constant $\lambda \approx 1.75 \times 10^{-24}$, non-linear case after 8 iterations.

So far we have used a damping constant of $\lambda \approx 1.175 \times 10^{-21}$. Before jumping to other inversion cases it is worth to investigate the effect of the choice of damping constant λ, due to the singularity of $M^{T*}M$ of equation (2.59). To demonstrate, first we considered slightly lower values than the chosen suitable damping constant λ. For $\lambda \approx 1.75 \times 10^{-24}$, the effect is shown in figure 4.10 and even after the band-pass filter shown in figure 4.11.

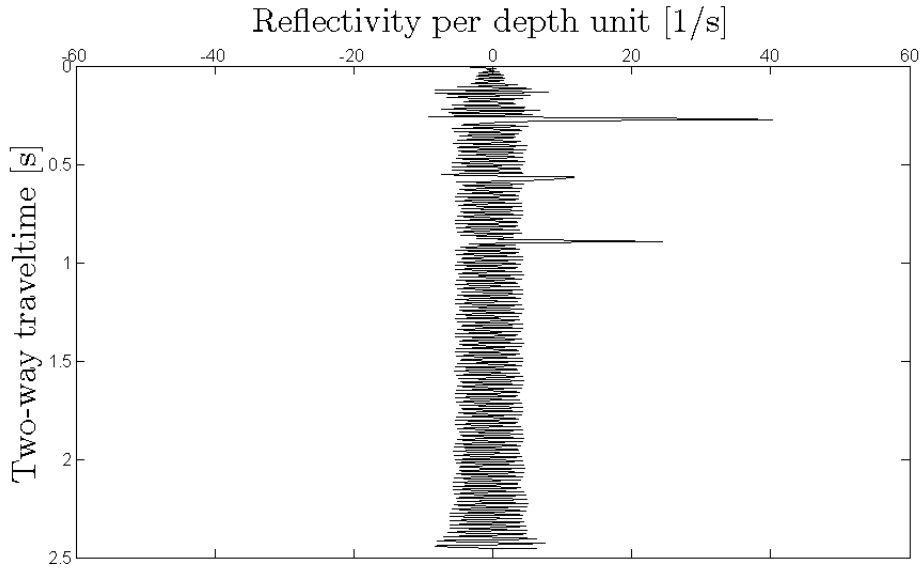

FIGURE 4.11: Inversion, $\lambda \approx 1.75 \times 10^{-24}$ plus band-pass filter, non-linear case after 8 iterations.

As we keep on taking smaller damping constant value, the matrix $M^{T*}M + \lambda I$ is no longer invertible. On the other hand, for the same model setup and $\lambda \approx 1.75 \times 10^{-8}$ the amplitude of the reflectivity per depth unit series shown in figure 4.12 gets smaller and the noise disappears. It is, therefore, found in this thesis that care should be taken in choosing the right damping constant λ in order to perform the inversion while maintaining the noise level and preserving the amplitude as much as possible.

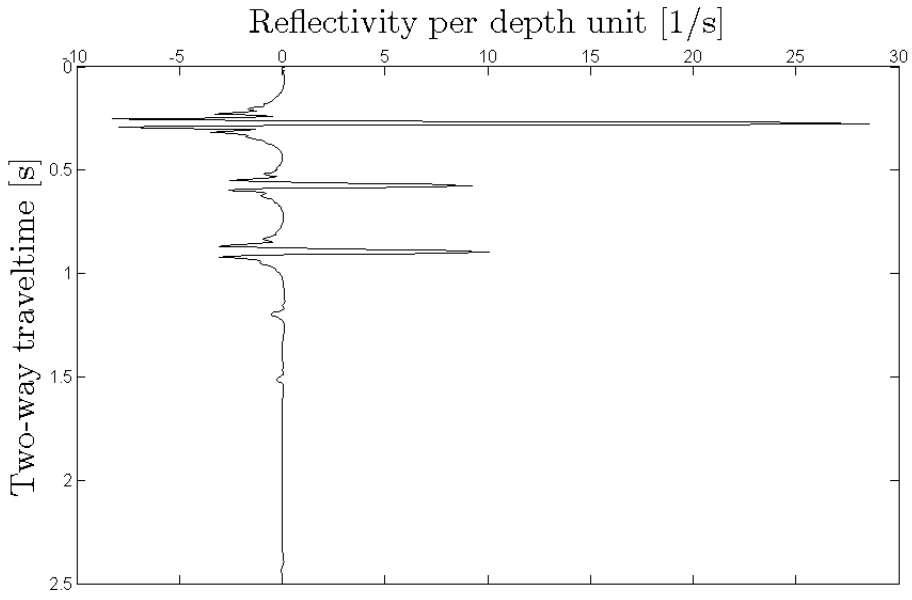

FIGURE 4.12: Inversion, $\lambda \approx 1.75 \times 10^{-8}$ without band-pass filter, non-linear case after 8 iterations.

Up on exploring the effects of the damping constant λ and the cut off frequency of the second order butterworth low pass band-filter used in this thesis, it is important to get the right balance between combination of both quantities not to compromise the amplitude and the dispersion corrections.

4.2 Inversion Using Wrong Q-Value

To see the effect of the quality factor Q in inversion process, a different Q-value or set of Q-values are used to generate the matrix M of equation (2.55) than that of the input synthetic seismogram $K(\omega, 0)$. Like the case of same Q-value, a second order butterworth low pass band-filter with cut-off frequency of $\frac{NT}{3} f_{Nqst}$ is used to remove the noise that appears after inversion. Thus, let us first consider inversion using larger Q value while the input synthetic seismogram $K(\omega, 0)$ is computed using a smaller Q-value. To do so, the input model parameters given in table (4.1) are used. The matrix M is computed using the quality factor sets of Q_2- and Q_3-values where as the input synthetic seismogram $K(\omega, 0)$ is computed using set Q_1. And, the resulted reflectivity per depth unit series $r(\tau)$ is shown in figures 4.13 and 4.14 respectively.

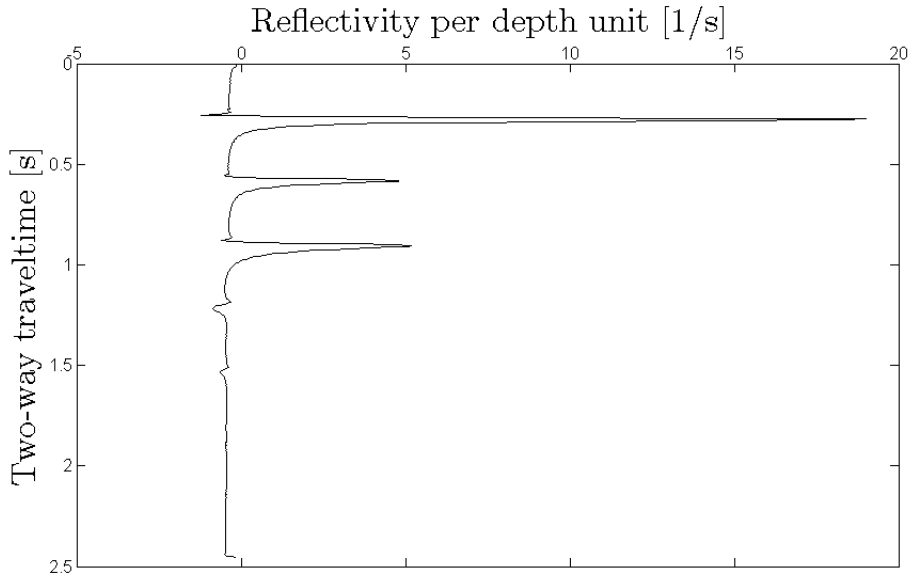

FIGURE 4.13: Inversion using a larger Q: Q_1 by Q_2, non-linear case after 8 iterations.

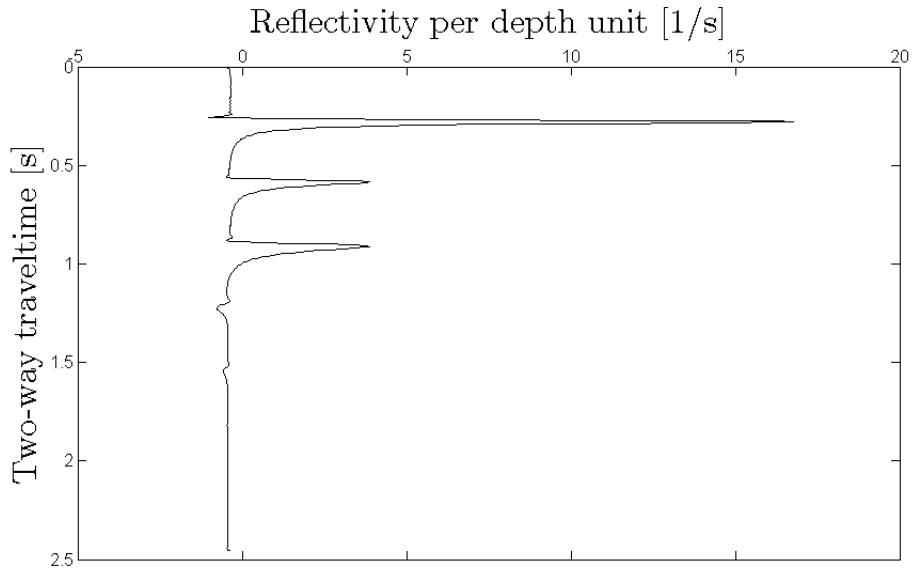

FIGURE 4.14: Inversion using a larger Q: Q_1 by $Q \approx \infty$, non-linear case after 8 iterations.

It can be seen from figures 4.5, 4.13 and 4.14 that the larger the quality factor Q used in inversion as compared to that of the input synthetic seismogram $K(\omega, 0)$, the smaller the amplitudes of the resulting reflectivity per depth unit series $r(\tau)$. This is because absorption is under-estimated and inverse Q filtering does not recover the high frequency energy completely.

Let us proceed with the second scenario whereby we have input synthetic seismogram $K(\omega, 0)$ calculated with large Q-value, sets Q_2 and Q_3, while now inversion is performed using smaller Q-value, set Q_1. The resulted reflectivity

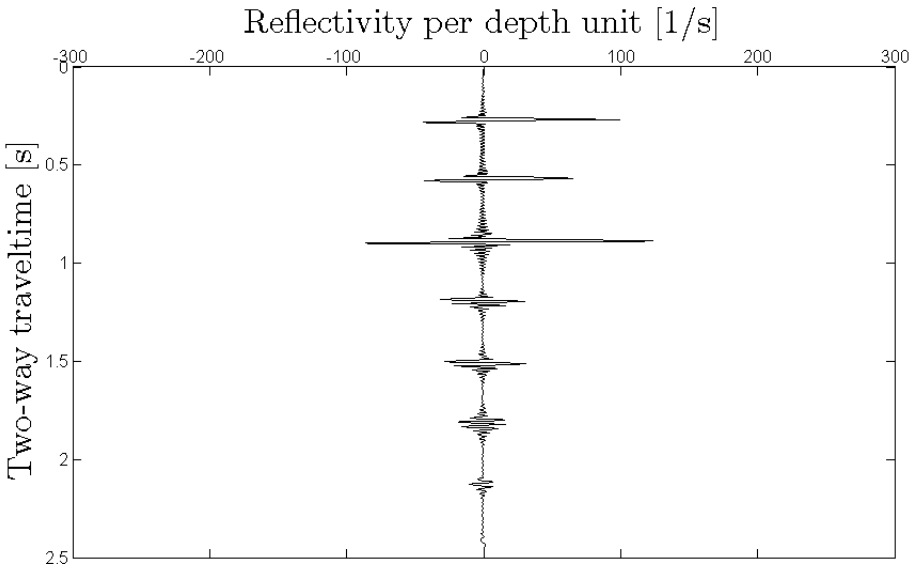

FIGURE 4.15: Inversion using a smaller Q: Q_2 by Q_1, non-linear case after 8 iterations.

per depth unit series $r(\tau)$ are shown in figures 4.15 and 4.16 respectively. We see that, inversion using a smaller Q-value as compared to the input seismogram results in more noise and does not show the true structure of the subsurface under study. This is because absorption is over-estimated and inverse Q filtering over-amplifies the high frequency energy. Therefore, comparing results of figures 4.15 and 4.16 with figures 4.5, 4.13 and 4.14, inversion using over-estimated Q-value is found to be better than using under-estimated Q-value.

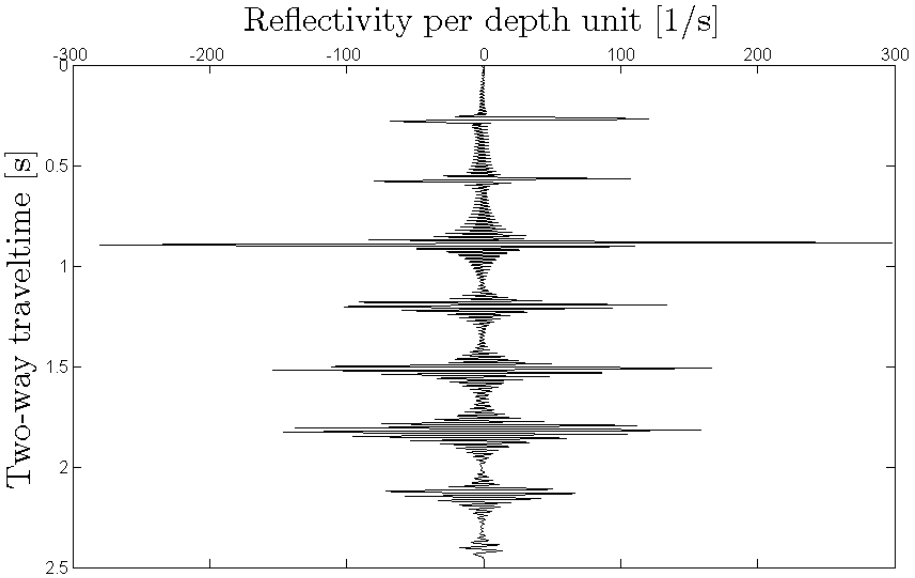

FIGURE 4.16: Inversion of absorption free medium ($Q \approx \infty$) by finite Q (Q_1), non-linear case after 8 iterations.

4.3 Effect of Q-Model on Inversion

So far to study the effect of the quality factor Q in the inversion process, the same Q-model was used to synthesize the input seismogram $K(\omega, 0)$ and the matrix M to do the inversion. Wang & Guo (2004*a*) Q-model of equation (3.7) has been used to do so. Now to see the effect of the Q-model, inversion using Wang & Guo (2004*a*) Q-model is performed while the input seismogram $K(\omega, 0)$ is synthesized using the alternative Futterman (1962) Q-model of equation (3.8), and vice versa. Again, a second order butterworth low pass band-filter with cut-off frequency of $\frac{NT}{3} f_{Nqst}$ is used to remove the noise that appears after inversion.

The same quality factor set Q_1-values given in table (4.1) is used both to compute the input synthetic seismogram $K(\omega, 0)$ and the matrix M to perform the inversion. The corresponding input synthetic seismograms $K(\omega, 0)$ are shown in figures 4.17 and 4.18 to help us understand the results of the inversion process. Though small, there is a slight difference in amplitude and shape of these synthesized input seismograms $K(\omega, 0)$. The difference between the two Q-models, as discussed in chapter 2, lies in the approximation of the velocity dispersion. Yet, the amplitude compensation remains the same. Though not significant, difference in wavelet shape is expected than in amplitude during the forward Q modelling of seismic wave $K(\omega, \tau)$.

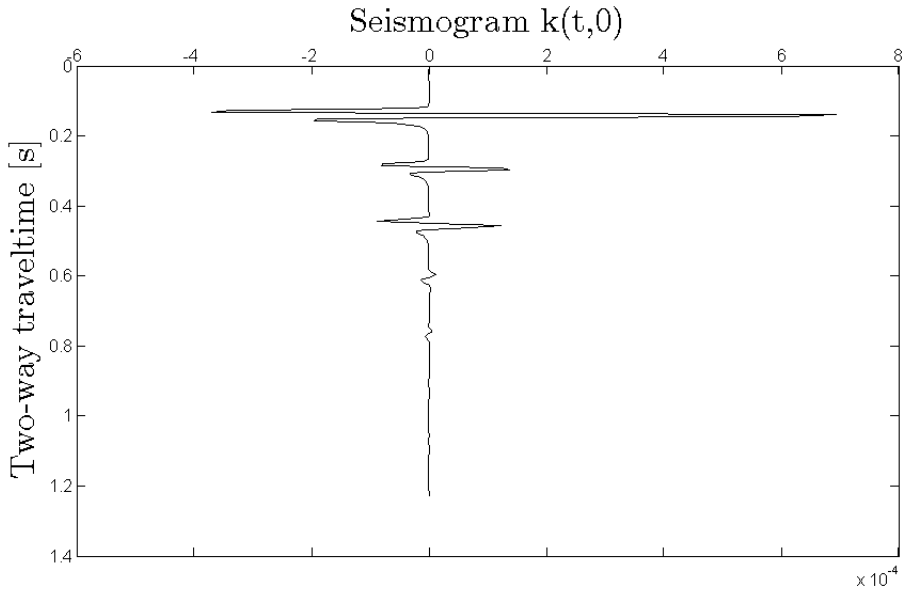

FIGURE 4.17: Seismogram $K(\omega, 0)$ synthesized using Wang & Guo (2004*a*) Q-model, non-linear case after 8 iterations.

Figure 4.19 shows the reflectivity per depth series $r(\tau)$ of an input seismogram $K(\omega, 0)$ is synthesized using Wang & Guo (2004*a*) Q-model and inversion by Futterman (1962) Q-model. And, the reversed scenario is shown in figure 4.20 where the input seismogram $K(\omega, 0)$ is synthesized using Futterman (1962) Q-model and inversion by Wang & Guo (2004*a*) Q-model.

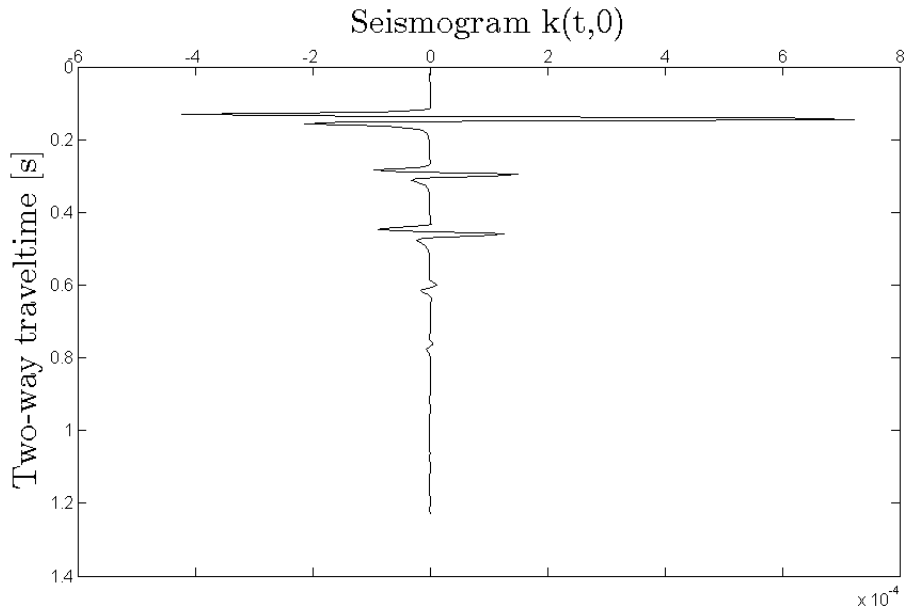

FIGURE 4.18: Seismogram $K(\omega, 0)$ synthesized using Futterman (1962) Q-model, non-linear case after 8 iterations.

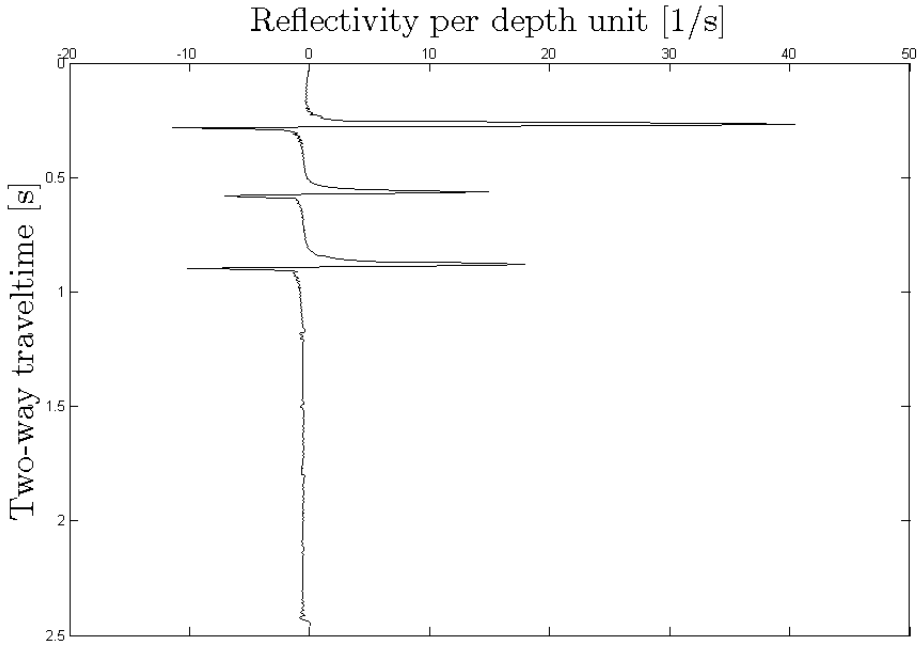

FIGURE 4.19: Inversion by Futterman (1962) Q-model, input $K(\omega, 0)$: figure 4.17.

Comparing figures 4.19 and 4.20 with figure 4.5, a case of same Q-model, show that the shape and amplitude of the resulting reflectivity per depth series $r(\tau)$ depend on the Q-model used when performing inversion of an input seismogram $K(\omega, 0)$ of a certain Q-model. As in the forward Q modelling of seismic wave $K(\omega, \tau)$, there is a significant difference in the shape of the resulting reflectivity per depth series $r(\tau)$ as a result of the inversion.

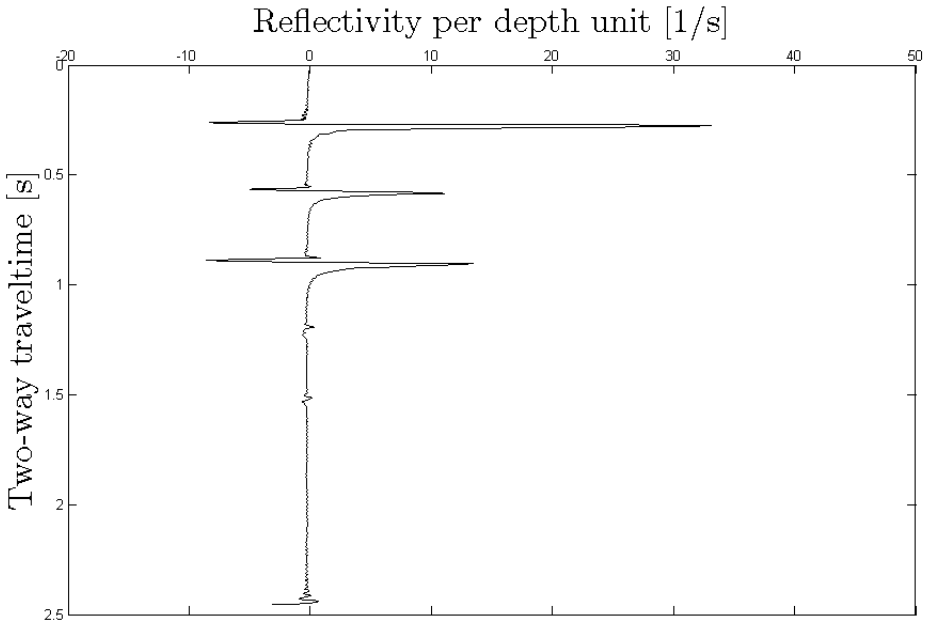

FIGURE 4.20: Inversion by Wang & Guo (2004*a*) Q-model, input $K(\omega, 0)$: figure 4.18.

Chapter 5

Discussion and Conclusion

In this thesis our main aim was to deal with compensation of absorption effects in seismic data by employing so-called inverse Q-filtering (IQF). This is a filtering technique that tries to restore the loss of higher frequencies due to propagation. It helps to improve the resolution of seismic data, and to balance the frequency contents.

The stability of inverse Q filtering, based on downward wave propagation, is always affected by high frequency noise whether it is implemented in time or frequency domain. Formulating the absorption compensation as an inverse problem, and solving the inverse problem iteratively, the resolution of seismic data is upgraded step by step. This inverse scheme helps to overcome the instability problem which is a natural drawback of common inverse Q filtering.

In this thesis work, a non-linear inverse Q filtering algorithm is derived starting with the introduction of absorption function $Y(\omega, \tau)$ into the stress-strain relationship and solving the wave propagation equation with finite difference method. Using forward Q modelling, of stratified (vertically inhomogeneous, horizontally layered, i.e., 1D) media, a synthetic seismogram is produced. The amplitude attenuation and wavelet broadening is demonstrated by varying the input Q-values. Moreover, the effect of the selected Q-model on the shape and amplitude of the synthesized seismogram is analyzed.

Using the forward synthetic seismogram as input, inversion is performed. Different scenarios like effects of Q-value (wrong Q-value) and Q-model on the inversion processing are investigated. It was found that using over estimated Q-values ($Q \Longrightarrow \infty$) during inversion resulted in reasonable reflectivity per depth unit series $r(\tau)$ rather than under estimated Q-values ($Q \Longrightarrow 0$). On the other hand, we found that use of under-estimated Q-values tend to amplify too much the recovered impulses and not preserve the relatives amplitudes. Yet, use of both under- and over-estimated Q-values result in change in shape of wavelet. These results prove that larger Q-values compensate part of the lost energy. Meanwhile smaller Q-vales over-compensate the high frequencies, and thus, the compensated result looks like strong high frequency noise. These observations found to be similar to the work done by, Oliveira & Lupinacci (2013).

Up selection of Q-model during inversion process, though not that significate, we observed that dispersion effects are more prominent rather than amplitude effects. This is because Q-models differ only in the velocity dispersion assumptions. Finally, it is found that the inversion method can be applied successfully to compute the variation of acoustic impedance $AI(\tau)$ given the acoustic impedance of the first infinitesimal thickness $\triangle\tau$ is known.

It would be interesting to test the developed inversion method to field data from structures with nearly plane and parallel stratification. The challenge will then be to find the complex reflection $K(\omega, 0)$ response of the layers. It would also be interesting to expand the method to non-vertical incidence.

Appendix

Forward Q Filter Modelling: This script prompts the user for the number of layer N and calculates the acoustic impedance $AI(\tau)$, reflectivity series $R(\tau)$ and reflectivity per depth unit series $r(\tau)$ of a model of N layers by reading input parameters: layer thickness z, velocity v, density ρ and quality factory Q from file 'model parameters'. Finally computes the synthetic seismogram $K(\omega, 0)$ at the surface.

Inversion: This script prompts the user for the number of layer N and calculates the reflectivity per depth unit series $r(\tau)$ by reading input: synthetic seismogram $K(\omega, 0)$ from the forward modelling and quality factory Q from file 'model parameters'. Finally computes the acoustic impedance $AI(\tau)$ and reflectivity series $R(\tau)$ from the reflectivity per depth unit series $r(\tau)$.

```
%% Model parameters
% Z = layer thickness in meter (m)
% rho = layer density in gram per cubic centimetre (g/cm3)
% v = layer velocity in meter per second (m/s2)
% Q = quality factor dimensionless

Z = [200,300,400,500];
% Z = [1800,900,450,150];

rho = [1,1.5,1.7,2.2];

v = [1500,2000,2500,3000];

% Q = [20,20,20,20];

Q = [20,25,30,35];
% Q = [40,50,60,70];
% Q = [60,75,90,105];
% Q = [80,100,120,140];
% Q = [100,125,150,175];
% Q = [200,250,300,350];
% Q = [400,500,600,700];
```

```
%% Forward Q Filter Modelling

% This script computes: acoustic impedance, reflectivity per depth unit series

% Finally compute the synthetic seismogram K(t,0)

N = input('Please enter the number of layers N: ');

Qmodel = input('Qmodel: 11 = Dispersionless, 12 = Wang, 13 = Futterman: ');
% Dispersion Q model

iflag = input('iflag: 2 = linear, 1 = non-linear, 0 = + free surface multiples: ');
% Linear and non-linear modelling

j = 1:1:N;

modelparameters;
% Specified input parameters

dt = 0.004;
% Sampling time

for j = 1:N

I(j) = rho(j).*v(j);
% Acoustic impedance of each layer

end

for jj = 1:N-1

   d(jj) = rho(jj+1).*v(jj+1) - rho(jj).*v(jj);
   s(jj) = rho(jj+1).*v(jj+1) + rho(jj).*v(jj);

   Rc(jj) = d(jj)./s(jj);
% Reflection coefficient of each interface

   Rs(jj) = (I(jj+1)./I(jj) - 1)/(2*dt);
% Reflectivity per depth unit of each interface

end
```

```
%% Now parametrizing in two way traveltime

tau(1) = 2*(Z(1)./v(1));
% Two way traveltime of the first interface

Ntau(1) = round(tau(1)/dt)+1;
% tau(k) = (k-1)dt where k = 1 surface.
% Corresponding number of samples

for k = 1:N-1

tau(k+1) = 2*(Z(k+1)./v(k+1)) + tau(k);
% Depth of each interface from the surface

Ntau(k+1) = Ntau(k) + round((2/dt)*(Z(k+1)./v(k+1)));
% Corresponding number of time steps

end

TM = tau(N);
% Model thickness in two way traveltime (TM)

NTM = Ntau(N);
% Corresponding number of time steps (NTM)

NT = 2*(NTM + 1);
% To avoid alaising, number of samples NT > 2*NTM

df = 1/(dt*NT);
% Sampling frequency

T = dt*NT;
% Maximum sampling time

fc = 20;
% Center frequency
```

```
%% Now sampling AI, Q, Rc & Rs in two way traveltime

    m = 1:NT;

for m = 1:Ntau(1)

    q(m) = Q(1);
   AI(m) = I(1);

end
for kk = 1:N-1

for m = Ntau(kk)+1:Ntau(kk+1)

    q(m) = Q(kk+1);
   AI(m) = I(kk+1);

end

end
for m = Ntau(N)+1:NT

    q(m) = Q(N);
   AI(m) = I(N);

end

rs(NT) = zeros;
rc(NT) = zeros;

for mm = 1:N-1

rs(Ntau(mm)) = Rs(mm);
rc(Ntau(mm)) = Rc(mm);

end
```

```
%% Compute K(omega,tau) using Ricket-wavelet

  NITR = 5;
   rsb = 0.5;
   % reflection coeff. for seafloor

   Tau = 74*dt;
   % vertical twt in water

     K = zeros(NT,NT);


if iflag == 2

   NITR = 1;

elseif iflag ==1 &&  iflag == 0

           NITR = 5;

end


% Hilbert Transform for Casual Futterman

     l = (-NT/2)+1:NT/2;
  frqq = l*df;
omegaa = 2.*pi.*frqq;

     H = imag(hilbert(-abs(omegaa)));

for ll = 1:NT

    for m = 1:NT

        X(ll,m) = (1./(2.*q(m))).*H(ll);

    end

end
```

```
for ii = 2:NT/2

      frq = (ii-1)*df;
    omega = 2.*pi.*frq;
     frqh = 125;
    coeff = (frqh/frq);

      srw = (2./sqrt(pi))*(frq^2/fc^3)*exp(-(frq/fc)^2);

 for nn = 1:NITR

     for m = 1:NT;

          if  Qmodel == 11 % Dispersionless

               Y(ii,m) = 1. - 1i./(2.*q(m));

          elseif  Qmodel == 12 % Modified Kolsky, Wang

               Y(ii,m) = coeff.^(1./(pi.*q(m))).*(1. - 1i./(2.*q(m)));

          else % Qmodel == 13 % Causal Futterman

           Y(ii,m) = (1. + (1./omega).*X(ii+(NT/2),m)) - 1i./(2*q(m));

          end

      end

        Phase(ii,NT) = -1i*omega*dt*Y(ii,NT)*(NT-1);
                  s1 = rs(NT)*exp(Phase(ii,NT));
                  sa = 0;

        for j = NT-1:-1:1

           Phase(ii,j) = -1i*omega*dt*Y(ii,j)*(j-1);
                 Ksqr = K(ii,j)*K(ii,j);
                   s2 = rs(j)*exp(Phase(ii,j))*(1.-Ksqr/srw^2);
                   sa = 0.5*dt*(s1+s2)+sa;
               K(ii,j) = sa*exp(-Phase(ii,j))*srw; %K(omega,tau)
                   s1 = s2;

        end

  end

end
```

```
%% Compute seismogram K(t,0)

S(1)= 0; % srw(1) = 0

% Fill in negative frequencies and include free-surface multiples

for nn = 2:NT/2

    S(nn) = K(nn,1);

    if iflag == 0

       fct = rsb*exp(-1i*2.*pi*(nn-1)*df*Tau);
       fct = 1/(1+fct);
     S(nn) = S(nn)*fct;

    end

  S(NT-nn+2) = conj(S(nn));

end

% Nyquist

  S(NT/2+1) = 0;

% Inverse FFT

 t = ifft(S,NT/2);
tt = dt:dt:T/2;
figure, plot(real(t(1:NT/2)),tt,'k')
set(gca,'YDir','reverse');
set(gca, 'XAxisLocation', 'top');
```

```
% Inversion

%% Input seismogram: Synthetic or real seismic data

ForwardQFilterModelling;

 INPUT(1,1)= 0; % srw(1) = 0

for nn = 2:NT/4

        INPUT(nn,1) = K(nn,1);

  INPUT(NT-nn+2,1) = conj(INPUT(nn,1));

end
```

```
%% Performing inversion with model parameters

ForwardQFilterModelling;

% Creating a matrix of NT X NT

  Knew = zeros(NT,NT);

for jj = 1:NITR;


    for nn = 2:NT/4

        frq = (nn-1)*df;
      omega = 2.*pi*frq;

        srw = (2./sqrt(pi))*(frq^2/fc^3)*exp(-(frq/fc)^2);

     Phase(nn,NT) = -1i*omega*dt*Y(nn,NT)*(NT-1);
    Matrix(nn,NT) = dt*exp(Phase(nn,NT))*srw;


          for m = NT-1:-1:1

       Phase(nn,m) = -1i*omega*dt*Y(nn,m)*(m-1);
           Knewsqr = Knew(nn,m)*Knew(nn,m);
      Matrix(nn,m) = dt*exp(Phase(nn,m))*(1.-Knewsqr/srw^2)*srw;

          end


    end
```

```
% Compute

mm = 1:1:NT;

FullMatrix(1,mm)= 0; % srw(1) = 0

 % Fill in negative frequencies

 for nn = 2:NT/4

    FullMatrix(nn,mm) = Matrix(nn,mm);
    FullMatrix(NT-nn+2,mm) = conj(FullMatrix(nn,mm));

end


% Least squares

lambda = svd((FullMatrix')*FullMatrix);
%  figure, plot(lambda)

% Generate damping matrix

for i = 1:NT

    for j = 1:NT

        if i==j

          Damp(i,j) = (1e4)*lambda(NT/2);
%           Damp(i,j) = lambda(NT/2);

        else

            Damp(i,j) = 0;

        end

    end

end
```

```
% Computing reflectivity per depth unit series

R = (((FullMatrix')*FullMatrix)+Damp)\((FullMatrix')*INPUT);

% Updating with new reflectivity per depth unit series

U = zeros(NT,NT);

for nn = 2:(NT/2)

    frq = (nn-1)*df;
    omega = 2.*pi*frq;

    srw = (2./sqrt(pi))*(frq^2/fc^3)*exp(-(frq/fc)^2);

     for ii = 1:NITR

         PHASE(nn,NT) = -1i*omega*dt*Y(nn,NT)*(NT-1);
                   S1 = R(NT)*exp(PHASE(nn,NT));
                   Sa = 0;

         for m = NT-1:-1:1

            PHASE(nn,m) = -1i*omega*dt*Y(nn,m)*(m-1);
                   Usqr = U(nn,m)*U(nn,m);
                     S2 = R(m)*exp(PHASE(nn,m))*(1.-Usqr/srw^2);
                     Sa = 0.5*dt*(S1+S2)+Sa;
                 U(nn,m) = Sa*exp(-PHASE(nn,m))*srw; %U(omega,tau)
                     S1 = S2;

         end

     end

end

Knew = U;

end
```

```
%% Compute seismogram K(t,0)

G(1)= 0; % srw(1) = 0

% Fill in negative frequencies and include free surface multiples

for nn = 2:NT/2

    G(nn) = U(nn,1);

    if iflag == 0

       fct = rsb*exp(-1i*2.*pi*(nn-1)*df*Tau);
       fct = 1/(1+fct);
     G(nn) = G(nn)*fct;

    end

    G(NT-nn+2) = conj(G(nn));

end

% Nyquist

G(NT/2+1)= 0;

% Inverse FFT

e = ifft(G,NT/2);
tt = dt:dt:T/2;
figure, plot(real(e),tt)
set(gca,'YDir','reverse');
set(gca, 'XAxisLocation', 'top');
```

```
%% Reflectivity series before band-pass filter

tt = dt:dt:T;
figure, plot(real(R),tt)
set(gca,'YDir','reverse');
set(gca, 'XAxisLocation', 'top');
```

```
%% Band-pass filter

n=2;
% 2nd order Butterworth filter

fnq=1/(2*dt);
% Nyquist frequency

flo = df;
fhi = NT*df/6;
% Wn=[flo/fnq fhi/fnq];
% Butterworth bandpass non-dimensional frequency

[b,a]=butter(n,fhi/fnq);
% construct the filter
% freqz(b,a)

Rfl=filtfilt(b,a,real(R));
% zero phase filter the data
```

```
%% Reflectivity series after band-pass filter

tt = dt:dt:T;
figure, plot(Rfl,tt)
set(gca,'YDir','reverse');
set(gca, 'XAxisLocation', 'top');
```

Bibliography

Aki, K. & Richards, P. G. (2002), *Quantitative Seismology.*, University Science Books, Sausalito, CA.

Barton, N. (2007), *ROCK QUALITY, SEISMIC VELOCITY, ATTENUATION AND ANISOTROPY*, Taylor & Francis/Balkema, AK Leiden, The Netherlands.

Bickel, S. H. & Natarajan, R. R. (1985), 'Plane Wave Q Deconvolution', *Geophysics* **50**(20), 1426–39.

Biot, M. A. (1956*a*), 'Theory of propagation of elastic waves in a fluid-saturated porous solid. I. Low-frequency range', *The Journal of the acoustical Society of America* **28**(2), 168–178.

Biot, M. A. (1956*b*), 'Theory of propagation of elastic waves in a fluid-saturated porous solid. II. Higher frequency range', *the Journal of the Acoustical Society of America* **28**(2), 179–191.

Cheng, P. & Margrave, G. F. (2011), 'Reflectivity modeling for stratified anelastic media', *CREWES Research Report* **23**.

Futterman, W. I. (1962), 'Dispersive body waves', *Journal of Geophysical Research* **67**(13), 5279–5291.

Gelius, L. J. (1987), 'Inverse Q-filtering. A spectral balancing technique', *Geophysical prospecting* **35**(6), 656–667.

Gelius, L. J. & Johansen, T. A. (2012), *PETROLEUM GEOPHYSICS, Second edition*, UniGEO as, Bergen, Norway.

Gjevik, B., Nilsen, A. & Höyen, J. (1976), 'An Attempt at the Inversion of Reflection DATA*', *Geophysical prospecting* **24**(3), 492–505.

Hale, D. (1982), 'Q-adaptive deconvolution', *Stanford Exploration Project* **30**, 133–158.

Hargreaves, N. D. & Calvert, A. J. (1991), 'Inverse Q filtering by Fourier transform', *Geophysics* **56**(4), 519–527.

Horton, C. W. (1959), 'A loss mechanism for the Pierre shale', *Geophysics* **24**(4), 667–680.

Jaeger, J. C. (1962), *Elasticity, fracture and flow with engineering and geological applications*, Methuen & Co. Ltd, London, UK.

Johnston, D. H., Toksöz, M. & Timur, A. (1979), 'Attenuation of seismic waves in dry and saturated rocks: II. Mechanisms', *Geophysics* **44**(4), 691–711.

Kjartansson, E. (1979), 'Constant Q-wave propagation and attenuation', *Journal of Geophysical Research: Solid Earth* **84**(B9), 4737–4748.

Klimentos, T. (1995), 'Attenuation of p-and s-waves as a method of distinguishing gas and condensate from oil and water', *Geophysics* **60**(2), 447–458.

Kolsky, H. (1956), 'LXXI. The propagation of stress pulses in viscoelastic solids', *Philosophical magazine* **1**(8), 693–710.

Mavko, G., Kjartansson, E. & Winkler, K. (1979), 'Seismic wave attenuation in rocks', *Reviews of Geophysics* **17**(6), 1155–1164.

Mavko, G. M. & Nur, A. (1979), 'Wave attenuation in partially saturated rocks', *Geophysics* **44**(2), 161–178.

Mitchell, B. J. & Hwang, H. (1987), 'Effect of low q sediments and crustal q on lg attenuation in the united states', *Bulletin of the Seismological Society of America* **77**(4), 1197–1210.

Montaña, C. A. & Margrave, G. F. (2004), 'Compensating for attenuation by inverse-q filtering', *CREWES Research Report* **16**.

Nilsen, A. & Gjevik, B. (1978), 'Inversion of Reflection Data*', *Geophysical Prospecting* **26**(2), 421–432.

Oliveira, S. A. M. & Lupinacci, W. M. (2013), 'L1 norm inversion method for deconvolution in attenuating media', *Geophysical Prospecting* **61**(4), 771–777.

Ricker, N. (1953), 'The form and laws of propagation of seismic wavelets', *Geophysics* **18**(1), 10–40.

Ricker, N. (1977), *Transient waves in visco-elastic media*, Vol. 10, Elsevier Scientific Publishing Company, Amsterdam, The Netherlands.

Robinson, J. C. (1979), 'A technique for the continuous representation of dispersion in seismic data', *Geophysics* **44**(8), 1345–1351.

Strick, E. (1967), 'The determination of Q, dynamic viscosity and transient creep curves from wave propagation measurements', *Geophysical Journal International* **13**(1-3), 197–218.

Telford, W. M., Geldart, L. P. & Sheriff, R. E. (1991), *Applied geophysics*, Vol. 1, Cambridge University Press.

van der Baan, M. (2012), 'Bandwidth enhancement: Inverse Q filtering or time-varying Wiener deconvolution?', *Geophysics* **77**(4), V133–V142.

Wang, Y. (2002), 'A stable and Efficient Approach to Inverse Q Filtering', *Geophysics* **67**, 1657–63.

Wang, Y. (2006), 'Inverse Q-filter for seismic resolution enhancement', *Geophysics* **71**(3), V51–V60.

Wang, Y. (2008), *Seismic Inverse Q Filtering*, Blackwell Publishing, Oxford, UK.

Wang, Y. & Guo, J. (2004*a*), 'Modified Kolsky model for seismic attenuation and dispersion', *Journal of Geophysics and Engineering* **1**(3), 187.

Wang, Y. & Guo, J. (2004*b*), 'Seismic migration with inverse Q$filtering', Geophysicalresearchletters$**31**(21).

White, J. (1975), 'Computed seismic speeds and attenuation in rocks with partial gas saturation', *Geophysics* **40**(2), 224–232.

Yilmaz, Ö. (2001), *Seismic Data Analysis: Processing, inversion, and interpretation of seismic data*, Society of Exploration Geophysicists Tulsa, Tulsa, USA.

Acknowledgements

Here I would like to give special thanks to my supervisors professor Leiv-J Gelius and professor Valerie Maupin for their support and assistance with the work done in this thesis. Without their help and guidance, this work would not have been possible. I would also like to thank the Department of Geosciences at the University of Oslo especially the Quota program for giving me the opportunity to study Geophysics.

...